



This is a repository copy of *Monopulse based DOA and polarization estimation with polarization sensitive arrays*.

White Rose Research Online URL for this paper:

<https://eprints.whiterose.ac.uk/183541/>

Version: Accepted Version

---

**Article:**

Dai, M., Ma, X., Liu, W. [orcid.org/0000-0003-2968-2888](https://orcid.org/0000-0003-2968-2888) et al. (3 more authors) (2022) Monopulse based DOA and polarization estimation with polarization sensitive arrays. *Signal Processing*, 195. 108487. ISSN 0165-1684

<https://doi.org/10.1016/j.sigpro.2022.108487>

---

Article available under the terms of the CC-BY-NC-ND licence (<https://creativecommons.org/licenses/by-nc-nd/4.0/>).

**Reuse**

This article is distributed under the terms of the Creative Commons Attribution-NonCommercial-NoDerivs (CC BY-NC-ND) licence. This licence only allows you to download this work and share it with others as long as you credit the authors, but you can't change the article in any way or use it commercially. More information and the full terms of the licence here: <https://creativecommons.org/licenses/>

**Takedown**

If you consider content in White Rose Research Online to be in breach of UK law, please notify us by emailing [eprints@whiterose.ac.uk](mailto:eprints@whiterose.ac.uk) including the URL of the record and the reason for the withdrawal request.



[eprints@whiterose.ac.uk](mailto:eprints@whiterose.ac.uk)  
<https://eprints.whiterose.ac.uk/>

# Monopulse Based DOA and Polarization Estimation with Polarization Sensitive Arrays

Minghui Dai<sup>a</sup>, Xiaofeng Ma<sup>a,\*</sup>, Wei Liu<sup>b</sup>, Weixing Sheng<sup>a</sup>, Yubing Han<sup>a</sup>, Huiwen Xu<sup>a</sup>

<sup>a</sup>*School of Electronic and Optical Engineering, Nanjing University of Science and Technology, Nanjing, China*

<sup>b</sup>*Department of Electronic and Electrical Engineering, University of Sheffield, S1 4BP Sheffield, U.K.*

---

## Abstract

In this paper, the vector sensor array (VSA) and the scalar sensor array (SSA) with polarization sensitivity (PS) are placed under the same framework of polarization sensitive arrays (PSAs), whose direction-dependent PS factor is larger than zero. **This commonality of their PS factors enables both VSA and SSA to perform polarization estimation effectively.** Based on this new PSA model, a generalized monopulse algorithm is proposed to jointly estimate direction-of-arrival (DOA) and polarization parameters, by expanding the existing monopulse angle estimation in spatial domain to both spatial and polarization domains. Both the DOA and polarization parameters can be effectively and efficiently estimated by comparing the outputs of the sum and spatial/polarized difference beams even with only one snapshot. Then, closed-form expressions for joint DOA and polarization estimation error variances are derived and the polarization estimation variance is proved to decrease monotonically with the PS factor. Simulations are carried out on an X-band 5x5 planar array composed of microstrip patch antennas to demonstrate the effectiveness of the proposed algorithm.

*Keywords:* Polarization sensitive arrays, joint DOA and polarization estimation, generalized monopulse method.

---

## 1. Introduction

The joint direction-of-arrival (DOA) and polarization estimation of electromagnetic (EM) sources has been widely studied in various applications, including radar, sonar, navigation and wireless communications [1, 2, 3, 4, 5]. Electromagnetic-vector-sensor (EMVS) is the most popular candidate to form polarization sensitive arrays (PSAs) [5, 6, 7, 8, 9, 10, 11]. Each EMVS is composed of several orthogonal electric and magnetic dipole elements to receive or transmit two or more orthogonal polarized signals simultaneously. Such PSAs with multiple-output antennas are also called vector sensor arrays (VSAs) [5]. Therefore, some dual-polarized antenna arrays, such as horizontal and vertical dual-polarized arrays [12], left-handed and right-handed circularly dual-polarized ones [13], are also VSAs.

Another kind of arrays with identical single-output antennas, called scalar sensor arrays (SSAs), is generally considered as polarization insensitive [14, 15, 16]. However, recent research indicates that the SSA has certain degree of polarization sensitivity (PS) [17]. Two orthogonal electric field components of all embedded elemental

---

\*Corresponding author

Email address: maxiaofeng@njust.edu.cn (Xiaofeng Ma)

antennas at different directions vary diversely under the mutual coupling (MC) effect. It makes the polarization characteristics of these embedded antennas deviating greatly from the isolated antenna element [18, 19, 20]. The polarization diversity from different directions of each antenna and the variations among all antennas enable a common SSA to have certain degree of PS. This PS in an SSA is *random* at different directions, but fixed when the antenna type and the array structure are determined.

Existing joint DOA and polarization estimation methods are normally designed for the VSAs composed of EMVSeSes, such as the vector cross product method in [5], the subspace-based methods in [21, 22, 23, 24], and the tensor-based method in [25]. Some computationally efficient methods are also proposed, such as the dimension-reduction MUSIC [26], the propagator-based method [27], and the quaternion-based method [28, 29]. However, joint DOA and polarization estimation based on the SSA with PS is rarely studied, except for our preliminary attempt in [30], where the dimension-reduction MUSIC is applied to separately estimate the DOA and polarization parameters, and the relationship between polarization estimation error variance and PS at different directions is briefly simulated without quantitative analysis.

The parameter estimation algorithms mentioned above are generally based on subspace multidimensional peak search, convex optimization, etc. On the other hand, the monopulse angle estimation technique can estimate DOA even with only one data snapshot by simply comparing the amplitude and phase difference of the simultaneously formed sum and difference beams [31, 32, 33]. The technique makes full use of the array gain with low computational cost and high estimation accuracy, hence it is widely used in practice for radar angle estimation and tracking of one target within the 3dB beamwidth of the sum beam. The monopulse technique has also been studied in polarimetric radar systems for enhanced DOA estimation [34, 35, 36, 37]. However, polarization estimation is performed only by simply comparing received signals from different polarized channels [36, 37, 38]. To the best of our knowledge, a generalized monopulse method for estimation of polarization parameters has not been available in literature yet.

There are three main contributions in this paper. Firstly, a PS factor  $z > 0$  is defined to unify both VSAs and SSAs under the framework of PSAs. Secondly, a GenerAlized Monopulse Estimation (GAME) algorithm for PSAs is derived, which extends the monopulse estimation technique from the spatial domain to both spatial and polarization domains. Thirdly, the covariance matrix for DOA and polarization estimation errors is derived, and the polarization estimation variance is rigorously proved to decrease monotonically with  $z$ .

The rest of this paper is organized as follows. The models for the SSA with PS and the VSA are introduced in Section II, followed by derivations of the GAME algorithm in Section III. The covariance matrix for the joint DOA and polarization estimation error and its relationship with the PS factor are derived in Section IV. The performance of the proposed method is demonstrated and analyzed in Section V and conclusions are drawn in Section VI.

Notations:  $(\cdot)^T$  stands for matrix/vector transpose, while  $(\cdot)^H$  denotes its Hermitian transpose. The operations  $\text{Re}(\cdot)$  and  $\text{Im}(\cdot)$  take the real and imaginary parts of a complex number, respectively.  $\mathbb{C}$  refers to the complex space. For a matrix,  $\text{diag}(\cdot)$  takes its diagonal elements, while for a vector, this operator constructs a diagonal matrix with elements in the vector.  $\mathbf{I}_M$  denotes the identity matrix of size  $M$ , while  $\mathbf{1}_M \in \mathbb{C}^{M \times 1}$  describes the

50 vector with all entries being one. For an array  $Y$ , the operators  $\min\{Y\}$  and  $\max\{Y\}$  mean to extract the smallest and largest number in the array respectively.  $\|\cdot\|$  denotes the joint complex Gaussian

## 2. Array Model

### 55 2.1. Polarization of EM Sig

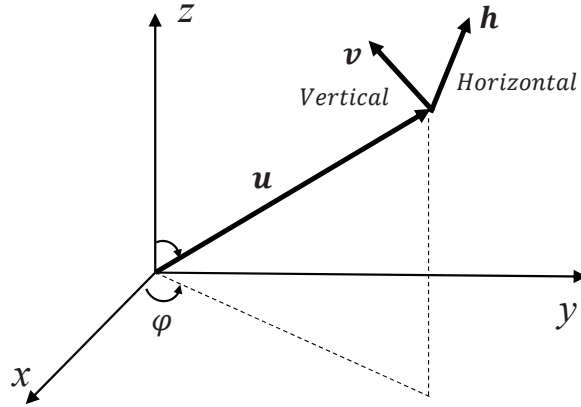


Figure 1: Orthonormal vector triad of an EM wave.

A planar EM wave received by an antenna array is composed of an electric field  $\mathbf{E}$  and a magnetic field  $\mathbf{H}$  that are orthogonal to the unit propagation direction vector  $\mathbf{u}(\theta, \varphi)$  shown in Fig. 1, where  $\theta \in [0, \pi/2]$  is the elevation angle and  $\varphi \in [0, 2\pi]$  is the azimuth angle. The relationship between  $\mathbf{E}$  and  $\mathbf{H}$  is

$$\mathbf{H} = -\frac{1}{\eta} \mathbf{u} \times \mathbf{E}, \quad (1)$$

where  $\eta$  is the intrinsic impedance of the medium. The electric and magnetic fields are orthogonal to each other and can be represented reciprocally [39]. Thus, the polarization of an EM wave is defined as the orientation of the electric field vector.

The vectors  $\mathbf{h}$  and  $\mathbf{v}$  in Fig. 1 are the horizontal and vertical polarized components of the electric field, respectively, which form a right-handed orthonormal basis [40].

$$\begin{aligned} \mathbf{u} &= [\sin \theta \cos \varphi, \sin \theta \sin \varphi, \cos \theta]^T \\ \mathbf{h} &= [-\sin \varphi, \cos \varphi, 0]^T \\ \mathbf{v} &= [\cos \theta \cos \varphi, \cos \theta \sin \varphi, -\sin \theta]^T \end{aligned} \quad (2)$$

The electric field vector of the incoming signal moves on an electric polarization ellipse, as shown in Fig. 2. The ellipse is described by the orientation angle  $\alpha \in (-\pi/2, \pi/2]$  and the ellipticity angle  $\beta \in (-\pi/4, \pi/4]$ . Then, the normalized electric vector  $\mathbf{E}$  can be expressed as

$$\mathbf{E} = \begin{bmatrix} E_h(t) & E_v(t) \end{bmatrix}^T = \mathbf{p}(\alpha, \beta) s(t) \quad (3)$$

where  $E_h(t)$  and  $E_v(t)$  are the horizontal and vertical electric fields, respectively, and  $s(t)$  denotes the transmitted scalar signal. The polarization characteristics of  $\mathbf{E}$  can be represented by the polarization vector  $\mathbf{p}(\alpha, \beta) \in \mathbb{C}^{2 \times 1}$  [41]

$$\mathbf{p}(\alpha, \beta) = \begin{bmatrix} \cos \alpha & -\sin \alpha \\ \sin \alpha & \cos \alpha \end{bmatrix} \begin{bmatrix} \cos \beta \\ j \sin \beta \end{bmatrix}. \quad (4)$$

As a result, an arbitrary polarization state can be uniquely represented by the polarization parameters  $\alpha$  and  $\beta$ . For example, the transmission is of linear polarization with  $\beta = 0$  and circular with  $|\beta| = \pi/4$ .

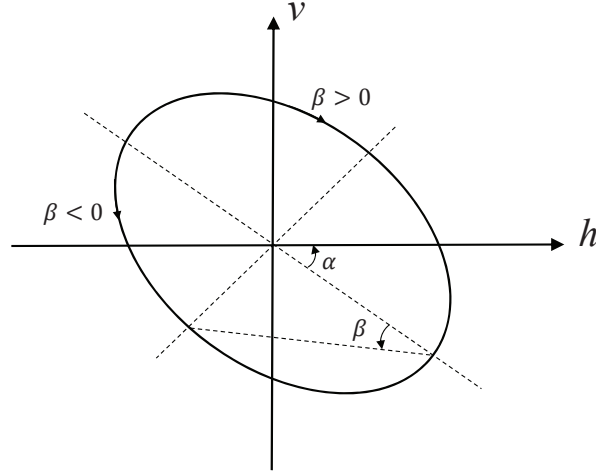


Figure 2: Polarization ellipse.

## 2.2. Scalar Sensor Array Model

Assume that  $K$  far-field stationary and narrowband signals from  $(\theta_k, \varphi_k)$  with polarization  $(\alpha_k, \beta_k)$  impinge on an array of  $M$  scalar sensors placed at locations  $\mathbf{r}_m = (x_m, y_m, z_m)$ ,  $m = 1, \dots, M$ ,  $K < M$ . The array output vector  $\mathbf{x}_{ssa}(t) \in \mathbb{C}^{M \times 1}$  is expressed as

$$\begin{aligned} \mathbf{x}_{ssa}(t) &= \sum_{k=1}^K \mathbf{a}_{ssa}(\theta_k, \varphi_k, \alpha_k, \beta_k) s_k(t) + \mathbf{n}_{ssa}(t) \\ &= \sum_{k=1}^K \mathbf{A}_{ssa}(\theta_k, \varphi_k) \cdot \mathbf{N} \cdot \mathbf{p}(\alpha_k, \beta_k) s_k(t) + \mathbf{n}_{ssa}(t) \end{aligned} \quad (5)$$

where  $\mathbf{n}_{ssa}(t) \in \mathbb{C}^{M \times 1}$  is the additive noise vector with zero mean and covariance matrix  $\sigma^2 \mathbf{I}_M$ ,  $\mathbf{a}_{ssa}(\theta_k, \varphi_k, \alpha_k, \beta_k) \in \mathbb{C}^{M \times 1}$  is the SSA spatial-polarization manifold vector and  $\mathbf{p}(\alpha_k, \beta_k)$  is the polarization vector of the  $k$ th signal  $s_k(t)$ .  $\mathbf{N} \in \mathbb{C}^{2 \times 2}$  is the feed network matrix of each scalar sensor, which combines the horizontal and vertical electric field components to form the desired polarization characteristic of each scalar sensor. For example, the scalar sensor is of right-handed circularly polarized antenna with  $\mathbf{N} = \text{diag}(1, -j)$  and left-handed circularly polarized with  $\mathbf{N} = \text{diag}(1, j)$ .  $\mathbf{A}_{ssa}(\theta_k, \varphi_k) \in \mathbb{C}^{M \times 2}$  is the spatial manifold matrix of the SSA, given by

$$\begin{aligned} \mathbf{A}_{ssa}(\theta_k, \varphi_k) &= \begin{bmatrix} \mathbf{A}_{h,ssa}(\theta_k, \varphi_k) & \mathbf{A}_{v,ssa}(\theta_k, \varphi_k) \end{bmatrix} \\ &= \mathbf{a}_S(\theta_k, \varphi_k) \odot \begin{bmatrix} \mathbf{f}_{h,ssa}(\theta_k, \varphi_k) & \mathbf{f}_{v,ssa}(\theta_k, \varphi_k) \end{bmatrix} \end{aligned} \quad (6)$$

where  $\mathbf{a}_S(\theta_k, \varphi_k) = [e^{jk_0 r_1 \mathbf{u}(\theta_k, \varphi_k)}, \dots, e^{jk_0 r_M \mathbf{u}(\theta_k, \varphi_k)}]^T \in \mathbb{C}^{M \times 1}$  is the spatial steering vector of the array with wavelength  $\lambda$  and wave number  $k_0 = 2\pi/\lambda$ .  $\mathbf{f}_{h,ssa}(\theta_k, \varphi_k) = [g_{h,1}(\theta_k, \varphi_k), \dots, g_{h,M}(\theta_k, \varphi_k)]^T$  and  $\mathbf{f}_{v,ssa}(\theta_k, \varphi_k) = [g_{v,1}(\theta_k, \varphi_k), \dots, g_{v,M}(\theta_k, \varphi_k)]^T$  are two orthogonal polarization components of the embedded antenna gain of  $M$  sensors for  $(\theta_k, \varphi_k)$ .  $g_{h,m}(\theta_k, \varphi_k)$  and  $g_{v,m}(\theta_k, \varphi_k)$  are the  $m$ th embedded antenna patterns of these two components.

Traditionally, as mentioned above, the antenna polarization characteristics are generally considered to be consistent among all elements in an SSA. In other words, there is no MC between array antennas, or the MC interaction has the same effect on the horizontal and vertical components. That is, the polarizations of all antennas in a specific direction are the same, given by

$$\frac{g_{v,m}(\theta_k, \varphi_k)}{g_{h,m}(\theta_k, \varphi_k)} = \gamma(\theta_k, \varphi_k), \quad m = 1, \dots, M \quad (7)$$

where  $\gamma(\theta_k, \varphi_k)$  is a complex constant. Then, the spatial manifold matrix in that direction is a rank-1 matrix.

$$\mathbf{A}_{ssa}(\theta_k, \varphi_k) = \mathbf{a}_S(\theta_k, \varphi_k) \odot \mathbf{f}_{h,ssa}(\theta_k, \varphi_k) \cdot [1 \quad \gamma(\theta_k, \varphi_k)] \quad (8)$$

It does not carry any polarization information, which means that the SSA is polarization insensitive.

However, the result will change when realistic MC effect between antennas is taken into consideration [19, 20]. In practical applications such as finite regular arrays or arrays with low sparsity, the MC has different effects on two electric field components of all antennas in each direction, which alters the polarization characteristic of the embedded antennas correspondingly. The polarization distinction varies among different antennas. This polarization diversity changes  $\mathbf{A}_{ssa}(\theta_k, \varphi_k)$  into a rank-2 matrix. The higher the polarization diversity is, the better the polarization estimation accuracy will be. The relevant proof will be given in Section IV.

The polarization diversity at direction  $(\theta_k, \varphi_k)$  of the SSA can be quantified by the PS factor  $z(\theta_k, \varphi_k)$ , defined as [17]

$$z(\theta_k, \varphi_k) = \frac{\sigma_2(\theta_k, \varphi_k)}{\sigma_1(\theta_k, \varphi_k)} \in [0, 1] \quad (9)$$

where  $\sigma_1(\theta_k, \varphi_k)$  and  $\sigma_2(\theta_k, \varphi_k)$  are the singular values of the matrix  $\mathbf{A}_{ssa}(\theta_k, \varphi_k)$ . As mentioned, the manifold matrix without MC does not contain any polarization information. Thus,  $\mathbf{A}_{ssa}(\theta_k, \varphi_k)$  is a rank-1 matrix for  $z(\theta_k, \varphi_k) = 0$ , while for  $z(\theta_k, \varphi_k) \neq 0$ ,  $\mathbf{A}_{ssa}(\theta_k, \varphi_k)$  becomes a rank-2 matrix with PS.

**Moreover**,  $z(\theta_k, \varphi_k)$  is direction-dependent. In this paper, the EM full-wave simulation software is employed to obtain the horizontal and vertical components,  $\mathbf{f}_{h,ssa}(\theta_k, \varphi_k)$  and  $\mathbf{f}_{v,ssa}(\theta_k, \varphi_k)$ , of all embedded active antennas to fully describe the polarization characteristic of the SSA.

### 2.3. Vector Sensor Array Model

Assume that each antenna of the VSA has  $J$  ( $J = 2$  to 6) orthogonal channels (e.g., crossed-dipole with  $J = 2$ , tripole with  $J = 3$ , and complete EMVS with  $J = 6$ ), the array output vector  $\mathbf{x}_{vsa}(t) \in \mathbb{C}^{JM \times 1}$  is expressed as

$$\begin{aligned} \mathbf{x}_{vsa}(t) &= \sum_{k=1}^K \mathbf{a}_{vsa}(\theta_k, \varphi_k, \alpha_k, \beta_k) s_k(t) + \mathbf{n}_{vsa}(t) \\ &= \sum_{k=1}^K \mathbf{A}_{vsa}(\theta_k, \varphi_k) \mathbf{p}(\alpha_k, \beta_k) s_k(t) + \mathbf{n}_{vsa}(t) \end{aligned} \quad (10)$$

where  $\mathbf{a}_{vsa}(\theta_k, \varphi_k, \alpha_k, \beta_k) \in \mathbb{C}^{JM \times 1}$  is the VSA spatial-polarization manifold vector and  $\mathbf{n}_{vsa}(t) \in \mathbb{C}^{JM \times 1}$  is the additive white Gaussian noise vector.  $\mathbf{A}_{vsa}(\theta_k, \varphi_k) \in \mathbb{C}^{JM \times 2}$  is the spatial manifold matrix, given by

$$\begin{aligned} \mathbf{A}_{vsa}(\theta_k, \varphi_k) &= \begin{bmatrix} \mathbf{A}_{h,vsa}(\theta_k, \varphi_k) & \mathbf{A}_{v,vsa}(\theta_k, \varphi_k) \end{bmatrix} \\ &= \mathbf{a}_S(\theta_k, \varphi_k) \otimes \mathbf{1}_J \odot \begin{bmatrix} \mathbf{f}_{h,vsa}(\theta_k, \varphi_k) & \mathbf{f}_{v,vsa}(\theta_k, \varphi_k) \end{bmatrix}. \end{aligned} \quad (11)$$

where  $\mathbf{f}_{h,vsa}(\theta_k, \varphi_k) = [g_{h,1}(\theta_k, \varphi_k), \dots, g_{h,JM}(\theta_k, \varphi_k)]^T$  and  $\mathbf{f}_{v,vsa}(\theta_k, \varphi_k) = [g_{v,1}(\theta_k, \varphi_k), \dots, g_{v,JM}(\theta_k, \varphi_k)]^T$  are two orthogonal polarization components of  $JM$  channels for  $(\theta_k, \varphi_k)$ .

For practical vector sensors whose channels are highly isolated to each other,  $\mathbf{f}_{h,vsa}^H(\theta_k, \varphi_k) \mathbf{f}_{v,vsa}(\theta_k, \varphi_k) = 0$ . Thus, according to the PS factor definition in (9) and the spatial manifold matrix  $\mathbf{A}_{vsa}$  in (11), the degree of PS for VSAs depends on the gain consistency of the two orthogonal electric field components  $\mathbf{A}_{h,vsa}(\theta_k, \varphi_k)$  and  $\mathbf{A}_{v,vsa}(\theta_k, \varphi_k)$  at different directions. The PS factor of the VSA can be expressed as

$$z(\theta_k, \varphi_k) = \frac{\sigma_2(\theta_k, \varphi_k)}{\sigma_1(\theta_k, \varphi_k)} = \sqrt{\frac{\min\{Y(\theta_k, \varphi_k)\}}{\max\{Y(\theta_k, \varphi_k)\}}} \quad (12)$$

where  $Y(\theta_k, \varphi_k) = \left\{ \mathbf{A}_{h,vsa}^H(\theta_k, \varphi_k) \mathbf{A}_{h,vsa}(\theta_k, \varphi_k), \mathbf{A}_{v,vsa}^H(\theta_k, \varphi_k) \mathbf{A}_{v,vsa}(\theta_k, \varphi_k) \right\}$ ,  $\sigma_1(\theta_k, \varphi_k)$  and  $\sigma_2(\theta_k, \varphi_k)$  are the singular values of  $\mathbf{A}_{vsa}(\theta_k, \varphi_k)$ . When the VSA is composed of ideal tripoles,  $J = 3$  and  $\mathbf{A}_{vsa}(\theta_k, \varphi_k)$  can be expressed as

$$\mathbf{A}_{vsa}(\theta_k, \varphi_k) = \mathbf{a}_S(\theta_k, \varphi_k) \otimes \mathbf{A}_r(\theta_k, \varphi_k) \quad (13)$$

where  $\mathbf{A}_r(\theta_k, \varphi_k) \in \mathbb{C}^{3 \times 2}$  is the response matrix of the tripoles [5]

$$\mathbf{A}_r(\theta_k, \varphi_k) = \begin{bmatrix} -\sin \varphi_k & \cos \theta_k \cos \varphi_k \\ \cos \varphi_k & \cos \theta_k \sin \varphi_k \\ 0 & -\sin \theta_k \end{bmatrix}. \quad (14)$$

The columns of  $\mathbf{A}_r(\theta_k, \varphi_k)$  are orthogonal. If there is no gain inconsistency among three dipoles,  $z(\theta_k, \varphi_k) = 1$  holds at all directions, i.e., the VSA composed of ideal tripoles is completely polarization sensitive.

### 90 3. Generalized Monopulse Estimation Algorithm

Compared with the subspace-based angle estimation method, the monopulse method is commonly employed in DOA estimation and tracking scenarios where the target position is roughly known [31, 32, 33]. In this section, the existing monopulse method will be firstly reviewed. Then, it is extended to the joint spatial and polarization domains to achieve low-complexity, high-precision joint-angle-and-polarization estimation, called the 95 GAME algorithm.

#### 3.1. Review of the Monopulse Method

The monopulse method is based on the maximum likelihood (ML) principle and mainly designed for the single target scenario, i.e.,  $K = 1$ . Then, the array output of (5) can be expressed as

$$\mathbf{x}_{ssa} = \mathbf{a}(\theta_t, \varphi_t) s + \mathbf{n}_{ssa} \quad (15)$$

where  $(\theta_t, \varphi_t)$  represents the target direction and  $\mathbf{a}(\theta_t, \varphi_t) = \mathbf{a}_S(\theta_t, \varphi_t)$ . The ML estimator maximizes the Gaussian density function  $p(\mathbf{x}_{ssa}; \theta_t, \varphi_t, s) = (1/(\pi\sigma^2)^M) e^{-(\mathbf{x}_{ssa} - \mathbf{a}(\theta_t, \varphi_t)s)^H (\mathbf{x}_{ssa} - \mathbf{a}(\theta_t, \varphi_t)s) / \sigma^2}$  with respect to the unknown parameters  $\theta_t, \varphi_t, s$  and the sample data vector  $\mathbf{x}_{ssa}$  [31]. It is noted that both the array polarization and the target polarization are commonly considered fixed and matched with each other in existing monopulse literature. Maximizing  $p(\mathbf{x}_{ssa}; \theta_t, \varphi_t, s)$  directly gives the ML estimation of  $s$

$$\begin{aligned} \hat{s} &= (\mathbf{a}^H(\theta_t, \varphi_t) \mathbf{a}(\theta_t, \varphi_t))^{-1} \mathbf{a}(\theta_t, \varphi_t)^H \mathbf{x}_{ssa} \\ &= \mathbf{a}^H(\theta_t, \varphi_t) \mathbf{x}_{ssa} / M \end{aligned} \quad (16)$$

which can be seen as the normalized output of the sum beam in direction  $(\theta_t, \varphi_t)$  in the case that the weight vector of the sum beam equals the steering vector of the target. Then, the target direction can be estimated by maximizing the power of the sum beam scan pattern

$$P(\theta, \varphi) = |\mathbf{a}^H(\theta, \varphi) \mathbf{x}_{ssa}|^2 \quad (17)$$

which is nonlinear in  $\theta$  and  $\varphi$ . If we maximize the function  $F(\theta, \varphi) = \ln P(\theta, \varphi)$ , we can obtain an approximation in the form of a linear equation by Taylor series expansion.

Assuming that the target direction  $(\theta_t, \varphi_t)$  is close to the sum beam direction  $(\theta_0, \varphi_0)$ , i.e.,  $F(\theta_t, \varphi_t) \approx F(\theta_0, \varphi_0)$ . The monopulse formula is approximately written in the form of the derivative of  $F(\theta, \varphi)$  in a first order Taylor series at  $(\theta_t, \varphi_t)$

$$\begin{pmatrix} \theta_t \\ \varphi_t \end{pmatrix} \approx \begin{pmatrix} \theta_0 \\ \varphi_0 \end{pmatrix} - \begin{pmatrix} F_{\theta\theta} & F_{\theta\varphi} \\ F_{\varphi\theta} & F_{\varphi\varphi} \end{pmatrix}_{(\theta_t, \varphi_t)}^{-1} \begin{pmatrix} F_\theta \\ F_\varphi \end{pmatrix}_{(\theta_0, \varphi_0)} \quad (18)$$

where  $F_\theta$  and  $F_\varphi$  are the first derivatives of  $F(\theta, \varphi)$ , known as monopulse ratio.

$$F_\rho = 2\text{Re}\{\mathbf{a}_{\rho,0}^H \mathbf{x}_{ssa} / \mathbf{a}_0^H \mathbf{x}_{ssa}\}, \rho = \theta, \varphi. \quad (19)$$

$F_{xy}$  is the second derivative of  $F(\theta, \varphi)$ , called monopulse slope.

$$\begin{aligned} F_{xy} &\approx (\mathbf{a}_{x,0}^H \mathbf{a}_{y,0} + \mathbf{a}_{y,0}^H \mathbf{a}_{x,0} \\ &+ \frac{\mathbf{a}_{x,0}^H \mathbf{a}_0 \mathbf{a}_0^H \mathbf{a}_{y,0} + \mathbf{a}_{y,0}^H \mathbf{a}_0 \mathbf{a}_0^H \mathbf{a}_{x,0}}{\mathbf{a}_0^H \mathbf{a}_0}) \Big/ \mathbf{a}_0^H \mathbf{a}_0, \quad x, y = \theta, \varphi \end{aligned} \quad (20)$$

when the weight vectors of the sum and difference beams are  $\mathbf{a}_0 = \mathbf{a}(\theta_0, \varphi_0)$  and  $\mathbf{a}_{x,0} = \frac{\partial \mathbf{a}_0}{\partial x} \Big|_{(\theta, \varphi) = (\theta_0, \varphi_0)}$ , respectively. In this case,  $F_{\theta\varphi} = F_{\varphi\theta} = 0$ .

In general, the weight vectors are optimized for low sidelobes or arbitrary beam pattern by amplitude tapering or pattern synthesis, etc., instead of using the steering vector directly. In such cases, a generalized monopulse angle estimation formula can be employed [42]

$$\begin{pmatrix} \theta_t \\ \varphi_t \end{pmatrix} \approx \begin{pmatrix} \theta_0 \\ \varphi_0 \end{pmatrix} - \begin{pmatrix} F_{\theta\theta} & F_{\theta\varphi} \\ F_{\varphi\theta} & F_{\varphi\varphi} \end{pmatrix}^{-1} \begin{pmatrix} F_\theta - \mu_\theta \\ F_\varphi - \mu_\varphi \end{pmatrix} \quad (21)$$

The monopulse slope  $F_{xy}(x, y = \theta, \varphi)$  is calculated similar to (20) as

$$\begin{aligned} F_{xy} &\approx (\mathbf{w}_{\Delta x}^H \mathbf{a}_{y,0} + \mathbf{a}_{y,0}^H \mathbf{w}_{\Delta x} \\ &+ \frac{\mathbf{w}_{\Delta x}^H \mathbf{a}_0 \mathbf{w}_\Sigma^H \mathbf{a}_{y,0} + \mathbf{a}_{y,0}^H \mathbf{w}_\Sigma \mathbf{a}_0^H \mathbf{w}_{\Delta x}}{\mathbf{a}_0^H \mathbf{w}_\Sigma}) \Big/ \mathbf{w}_\Sigma^H \mathbf{a}_0, \quad x, y = \theta, \varphi \end{aligned} \quad (22)$$

where  $\mathbf{w}_\Sigma$  and  $\mathbf{w}_{\Delta x}$  represent the designed sum and difference beam weights, respectively.  $\mu_x = \text{Re} \{ \mathbf{w}_{\Delta x}^H \mathbf{a}_0 / \mathbf{w}_\Sigma^H \mathbf{a}_0 \}$  ( $x = \theta, \varphi$ ) in (21) is the bias correction term for all kinds of weights.

### 3.2. Generalized Monopulse Formula

If the target polarization is involved, the received EM wave of a single target can be written as

$$\mathbf{x} = \mathbf{a}(\theta_t, \varphi_t, \alpha_t, \beta_t) s + \mathbf{n} \quad (23)$$

where  $(\alpha_t, \beta_t)$  are target polarization parameters,  $\mathbf{a}(\theta_t, \varphi_t, \alpha_t, \beta_t) = \mathbf{A}(\theta_t, \varphi_t) \mathbf{p}(\alpha_t, \beta_t)$ .  $\mathbf{A}(\theta_t, \varphi_t) = \mathbf{A}_{ssa}(\theta_t, \varphi_t)$ ,  $\mathbf{x} = \mathbf{x}_{ssa}$ , and  $\mathbf{n} = \mathbf{n}_{ssa}$  for the SSA with PS, while  $\mathbf{A}(\theta_t, \varphi_t) = \mathbf{A}_{vsa}(\theta_t, \varphi_t)$ ,  $\mathbf{x} = \mathbf{x}_{vsa}$ , and  $\mathbf{n} = \mathbf{n}_{vsa}$  for the VSA. In the following derivation,  $\mathbf{a}(\theta_t, \varphi_t, \alpha_t, \beta_t)$  is simplified as  $\mathbf{a}$ .

Assume the polarization of the sum beam towards  $(\theta_0, \varphi_0)$  is  $(\alpha_0, \beta_0)$ , and then the generalized monopulse formula similar to (21) is

$$\boldsymbol{\rho} = \boldsymbol{\rho}_0 + \mathbf{C}(\hat{\mathbf{r}} - \boldsymbol{\mu}) \quad (24)$$

where  $\boldsymbol{\rho} = (\theta, \varphi, \alpha, \beta)^T$ ,  $\boldsymbol{\rho}_0 = (\theta_0, \varphi_0, \alpha_0, \beta_0)$ , and  $\boldsymbol{\mu} = (\mu_\theta \ \mu_\varphi \ \mu_\alpha \ \mu_\beta)^T$  is the bias correction vector. Moreover,

$$\mathbf{C} = \begin{pmatrix} c_{\theta\theta} & c_{\theta\varphi} & c_{\theta\alpha} & c_{\theta\beta} \\ c_{\varphi\theta} & c_{\varphi\varphi} & c_{\varphi\alpha} & c_{\varphi\beta} \\ c_{\alpha\theta} & c_{\alpha\varphi} & c_{\alpha\alpha} & c_{\alpha\beta} \\ c_{\beta\theta} & c_{\beta\varphi} & c_{\beta\alpha} & c_{\beta\beta} \end{pmatrix} \quad (25)$$

is a slope correction matrix and  $\hat{\mathbf{r}} = (\hat{r}_\theta \ \hat{r}_\varphi \ \hat{r}_\alpha \ \hat{r}_\beta)^T$  is the monopulse ratio vector obtained from the outputs of sum and difference beams

$$\hat{r}_\rho = \text{Re}\{d_\rho/s_\Sigma\}, \rho = \theta, \varphi, \alpha, \beta \quad (26)$$

where  $s_\Sigma = \mathbf{w}_\Sigma^H \mathbf{x}$  and  $d_\rho = \mathbf{w}_{\Delta\rho}^H \mathbf{x}$  are the outputs of sum and difference beams, respectively. Moreover, in order to reduce the fluctuation of the single-snapshot monopulse ratio, the averaged monopulse ratio vector  $\hat{\mathbf{r}}_L$  is introduced [33]

$$\hat{\mathbf{r}}_L = \sum_{l=1}^L \mathbf{d}_l s_{\Sigma,l}^* / \sum_{l=1}^L |s_{\Sigma,l}|^2 \quad (27)$$

where  $s_{\Sigma,l}$  and  $\mathbf{d}_l = (d_{\theta,l}, d_{\varphi,l}, d_{\alpha,l}, d_{\beta,l})^T$  represent the  $l$ th ( $l = 1, 2, \dots, L$ ) snapshot of the sum and difference beam outputs.

Then,  $\boldsymbol{\mu}$  and  $\mathbf{C}$  can be determined when the expectation of parameter estimation error is unbiased, and the monopulse characteristic  $\mathbf{M}(\theta, \varphi, \alpha, \beta)$  is approximately a linear function of the target direction and polarization as [42]

$$\mathbf{M}(\theta, \varphi, \alpha, \beta) = \mathbf{C}(\text{E}\{\hat{\mathbf{r}}\} - \boldsymbol{\mu}) = \boldsymbol{\rho} - \boldsymbol{\rho}_0 \quad (28)$$

Thus, we have

$$\mathbf{M}(\theta_0, \varphi_0, \alpha_0, \beta_0) = 0 \quad (29)$$

$$\left. \frac{\partial \mathbf{M}}{\partial \theta} \right|_{\boldsymbol{\rho}=\boldsymbol{\rho}_0} = \begin{bmatrix} 1 & 0 & 0 & 0 \end{bmatrix}^T \quad (30a)$$

$$\left. \frac{\partial \mathbf{M}}{\partial \varphi} \right|_{\boldsymbol{\rho}=\boldsymbol{\rho}_0} = \begin{bmatrix} 0 & 1 & 0 & 0 \end{bmatrix}^T \quad (30b)$$

$$\left. \frac{\partial \mathbf{M}}{\partial \alpha} \right|_{\boldsymbol{\rho}=\boldsymbol{\rho}_0} = \begin{bmatrix} 0 & 0 & 1 & 0 \end{bmatrix}^T \quad (30c)$$

$$\left. \frac{\partial \mathbf{M}}{\partial \beta} \right|_{\boldsymbol{\rho}=\boldsymbol{\rho}_0} = \begin{bmatrix} 0 & 0 & 0 & 1 \end{bmatrix}^T \quad (30d)$$

Note that  $\mathbb{E}\{\hat{r}_\rho\}$  can be calculated by

$$\begin{aligned} \mathbb{E}\{\hat{r}_\rho\} &= \text{Re} \left\{ \frac{\mathbf{w}_{\Delta\rho}^H \mathbb{E}\{\mathbf{x}\mathbf{x}^H\} \mathbf{w}_\Sigma}{\mathbf{w}_\Sigma^H \mathbb{E}\{\mathbf{x}\mathbf{x}^H\} \mathbf{w}_\Sigma} \right\} \\ &\approx \frac{|s|^2 \text{Re}\{\mathbf{w}_{\Delta\rho}^H \mathbf{a}\mathbf{a}^H \mathbf{w}_\Sigma\} + \text{Re}\{\sigma^2 \mathbf{w}_{\Delta\rho}^H \mathbf{w}_\Sigma\}}{|s|^2 \mathbf{w}_\Sigma^H \mathbf{a}\mathbf{a}^H \mathbf{w}_\Sigma + \sigma^2 \mathbf{w}_\Sigma^H \mathbf{w}_\Sigma}, \rho = \theta, \varphi, \alpha, \beta \end{aligned} \quad (31)$$

Assume that the output noise powers of the sum and difference beams are both small and can be ignored, i.e.  $\sigma^2 \mathbf{w}_\Sigma^H \mathbf{w}_\Sigma \approx 0$ ,  $\sigma^2 \mathbf{w}_{\Delta\rho}^H \mathbf{w}_\Sigma \approx 0$ . Then,

$$\mathbb{E}\{\hat{r}_\rho\} = \frac{|s|^2 \text{Re}\{\mathbf{w}_{\Delta\rho}^H \mathbf{a}\mathbf{a}^H \mathbf{w}_\Sigma\}}{|s|^2 \mathbf{w}_\Sigma^H \mathbf{a}\mathbf{a}^H \mathbf{w}_\Sigma}, \rho = \theta, \varphi, \alpha, \beta \quad (32)$$

Subsequently,  $\boldsymbol{\mu} = (\mu_\theta \ \mu_\varphi \ \mu_\alpha \ \mu_\beta)^T$  can be determined according to (28) and (29) as

$$\mu_\rho = \mathbb{E}\{\hat{r}_\rho\}|_{\boldsymbol{\rho}=\boldsymbol{\rho}_0} = \text{Re} \left\{ \frac{\mathbf{w}_{\Delta\rho}^H \mathbf{a}_0}{\mathbf{w}_\Sigma^H \mathbf{a}_0} \right\}, \rho = \theta, \varphi, \alpha, \beta \quad (33)$$

where  $\mathbf{a}_0$  is the array spatial-polarization manifold vector when the target parameter matches with the sum beam, i.e.,  $\mathbf{a}_0 = \mathbf{a}(\theta_0, \varphi_0, \alpha_0, \beta_0)$ . Meanwhile, according to (28) and (30), the following formula holds

$$\mathbf{C} \left( \begin{array}{cccc} \frac{\partial \hat{r}}{\partial \theta} & \frac{\partial \hat{r}}{\partial \varphi} & \frac{\partial \hat{r}}{\partial \alpha} & \frac{\partial \hat{r}}{\partial \beta} \end{array} \right) \Big|_{\boldsymbol{\rho}=\boldsymbol{\rho}_0} = \mathbf{I}_4 \quad (34)$$

Thus, the elements of inverse slope correction matrix  $\mathbf{F} = \mathbf{C}^{-1}$  can be expressed as

$$\begin{aligned} F_{xy} &= \mathbb{E} \left\{ \frac{\partial \hat{r}_x}{\partial y} \right\} \Big|_{\boldsymbol{\rho}=\boldsymbol{\rho}_0} = \frac{\text{Re}\{\mathbf{w}_{\Delta x}^H \mathbf{a}_{y,0} \mathbf{a}_0^H \mathbf{w}_\Sigma + \mathbf{w}_{\Delta x}^H \mathbf{a}_0 \mathbf{a}_{y,0}^H \mathbf{w}_\Sigma\}}{\mathbf{w}_\Sigma^H \mathbf{a}_0 \mathbf{a}_0^H \mathbf{w}_\Sigma} \\ &\quad - \mu_x \frac{2\text{Re}\{\mathbf{w}_\Sigma^H \mathbf{a}_{y,0} \mathbf{a}_0^H \mathbf{w}_\Sigma\}}{\mathbf{w}_\Sigma^H \mathbf{a}_0 \mathbf{a}_0^H \mathbf{w}_\Sigma}, \quad x, y = \theta, \varphi, \alpha, \beta. \end{aligned} \quad (35)$$

110 where  $\mathbf{a}_{y,0}$  is the derivative of  $\mathbf{a}_0$  with respect to  $y$  ( $y = \theta, \varphi, \alpha, \beta$ ).

Therefore, after obtaining the bias correction vector from 33 and the slope correction matrix from 35, the DOA and polarization parameters can be directly estimated from 24.

In this paper, the weights of the sum and difference beams are assigned as the normalized spatial-polarization vector  $\bar{\mathbf{a}}_0$  with desired DOA  $(\theta_0, \varphi_0)$  and polarization  $(\alpha_0, \beta_0)$ , and its derivatives, respectively,

$$\bar{\mathbf{w}}_\Sigma = \bar{\mathbf{a}}_0 = \bar{\mathbf{A}}(\theta_0, \varphi_0) \mathbf{p}(\alpha_0, \beta_0) \quad (36a)$$

$$\bar{\mathbf{w}}_{\Delta\rho} = \left. \frac{\partial \bar{\mathbf{w}}_{\Sigma}}{\partial \rho} \right|_{\rho=\theta,\varphi,\alpha,\beta} \quad (36b)$$

where  $\bar{\mathbf{A}}(\theta, \varphi) = \mathbf{A}(\theta, \varphi) / \|\mathbf{A}(\theta, \varphi)\|$  is the normalized array manifold matrix. Then,  $F_{xy} = 0 (x \neq y)$  can be calculated by (35), and (24) can be rewritten as

$$\text{diag}(F_{\theta\theta}, F_{\varphi\varphi}, F_{\alpha\alpha}, F_{\beta\beta})(\boldsymbol{\rho} - \boldsymbol{\rho}_0) = \hat{\mathbf{r}} - \boldsymbol{\mu} \quad (37)$$

where the monopulse slope  $F_{\rho\rho}$  is determined by (35) as

$$F_{\rho\rho} = \frac{\text{Re}\{\bar{\mathbf{w}}_{\Delta\rho}^H \bar{\mathbf{w}}_{\Delta\rho} \bar{\mathbf{w}}_{\Sigma}^H \bar{\mathbf{w}}_{\Sigma} + \bar{\mathbf{w}}_{\Delta\rho}^H \bar{\mathbf{w}}_{\Sigma} \bar{\mathbf{w}}_{\Delta\rho}^H \bar{\mathbf{w}}_{\Sigma}\}}{\bar{\mathbf{w}}_{\Sigma}^H \bar{\mathbf{w}}_{\Sigma} \bar{\mathbf{w}}_{\Sigma}^H \bar{\mathbf{w}}_{\Sigma}} - \text{Re}\left\{\frac{\bar{\mathbf{w}}_{\Delta\rho}^H \bar{\mathbf{w}}_{\Sigma}}{\bar{\mathbf{w}}_{\Sigma}^H \bar{\mathbf{w}}_{\Sigma}}\right\} \cdot \frac{2\text{Re}\{\bar{\mathbf{w}}_{\Sigma}^H \bar{\mathbf{w}}_{\Delta\rho} \bar{\mathbf{w}}_{\Sigma}^H \bar{\mathbf{w}}_{\Sigma}\}}{\bar{\mathbf{w}}_{\Sigma}^H \bar{\mathbf{w}}_{\Sigma} \bar{\mathbf{w}}_{\Sigma}^H \bar{\mathbf{w}}_{\Sigma}}, \rho = \theta, \varphi, \alpha, \beta \quad (38)$$

#### 4. Performance Analysis

In this section, performance of the proposed GAME algorithm is analyzed in terms of monopulse ratio distribution. The covariance matrix for DOA and polarization estimations is subsequently derived, together with their relationships with the PS factor. Moreover, its computational complexity is compared with that of the dimension-reduction MUSIC algorithm in [30].

##### 4.1. Performance Evaluation Based on Monopulse Ratio Distribution

It is demonstrated in [31] that the mean and covariance of the estimator (24) is

$$\mathbb{E}\{\boldsymbol{\rho}\} = \boldsymbol{\rho}_0 - \mathbf{C}(\mathbb{E}\{\hat{\mathbf{r}}\} - \boldsymbol{\mu}) \quad (39a)$$

$$\text{cov}\{\boldsymbol{\rho}\} = \mathbf{C}\text{cov}\{\hat{\mathbf{r}}\} \mathbf{C}^T \quad (39b)$$

The vector form of beam outputs  $(\mathbf{d}^T, s_{\Sigma})$  is subject to the complex normal distribution with mean  $\mathbf{t}$  and covariance matrix  $\mathbf{G}$ , i.e.,  $(\mathbf{d}^T, s_{\Sigma})^T \sim CN(\mathbf{t}, \mathbf{G})$ . Let  $\mathbf{t}$ ,  $\mathbf{G}$  be partitioned according to the sum and difference beam parts as

$$\mathbf{t} = \begin{pmatrix} \mathbf{t}_D \\ \mathbf{t}_S \end{pmatrix} \quad (40a)$$

$$\mathbf{G} = \begin{pmatrix} \mathbf{G}_D & \mathbf{G}_{DS} \\ \mathbf{G}_{DS}^H & \mathbf{G}_S \end{pmatrix}. \quad (40b)$$

with

$$\mathbf{t}_D = \gamma \mathbf{W}_{\Delta\rho}^H \mathbf{a} \quad (41a)$$

$$\mathbf{t}_S = \gamma \mathbf{w}_{\Sigma}^H \mathbf{a} \quad (41b)$$

$$\mathbf{G}_D = \gamma^2 \mathbf{W}_{\Delta\rho}^H \mathbf{a} \mathbf{a}^H \mathbf{W}_{\Delta\rho} + \mathbf{W}_{\Delta\rho}^H \mathbf{W}_{\Delta\rho} \quad (41c)$$

$$\mathbf{G}_{DS} = \gamma^2 \mathbf{W}_{\Delta\rho}^H \mathbf{a} \mathbf{a}^H \mathbf{w}_\Sigma + \mathbf{W}_{\Delta\rho}^H \mathbf{w}_\Sigma \quad (41d)$$

$$G_S = \gamma^2 \mathbf{w}_\Sigma^H \mathbf{a} \mathbf{a}^H \mathbf{w}_\Sigma + \mathbf{w}_\Sigma^H \mathbf{w}_\Sigma \quad (41e)$$

where  $\mathbf{W}_{\Delta\rho} = \begin{pmatrix} \mathbf{w}_{\Delta\theta} & \mathbf{w}_{\Delta\varphi} & \mathbf{w}_{\Delta\alpha} & \mathbf{w}_{\Delta\beta} \end{pmatrix}$ ,  $\gamma^2 = \mathbb{E}\{|s|^2\} = 10^{\text{SNR}/10}$  denotes the power of the target, and SNR is the elemental signal-to-noise ratio.

Then, the first and second order statistical properties of  $\hat{\mathbf{r}}$  can be calculated by integrating over the distribution of  $s_\Sigma$  [33]. Assume the target is non-fluctuating, and then the mean and covariance of  $\hat{\mathbf{r}}$  conditioned on the sum beam power  $P_S = \sum_{l=1}^L |s_{\Sigma,l}|^2$  exceeding a detection threshold  $\delta$  are concluded as follows.

1. The conditional mean is

$$\begin{aligned} \mathbb{E}\{\hat{\mathbf{r}} | P_S > \delta\} &= \text{Re} \left\{ \mathbf{G}_{DS}/G_S + (t_D - \mathbf{G}_{DS}G_S^{-1}t_S) \right. \\ &\quad \left. \cdot \mathbb{E} \left( \sum_{l=1}^L S_l^H / \sum_{l=1}^L |S_l|^2 | P_S > \delta \right) \right\}. \end{aligned} \quad (42)$$

When  $L = 1$ , the analytic form is

$$\begin{aligned} \mathbb{E}\{\hat{\mathbf{r}} | P_S > \delta\} \\ = (A_m/P_D) \text{Re}\{\mathbf{G}_{DS}/G_S\} + (1 - A_m/P_D) \text{Re}\{t_D/t_S\} \end{aligned} \quad (43)$$

where  $P_D = \Pr\{P_S > \delta\}$  is the detection probability, and  $A_m$  is a constant related to the SNR [33]

$$\begin{aligned} P_D &= \int_\delta^\infty \frac{1}{G_S} \left( \frac{t}{L|t_S|^2} \right)^{(L-1)/2} e^{-(t+L|t_S|^2)/G_S} \\ &\quad \cdot \mathbf{I}_{L-1}(2\sqrt{tL}|t_S|/G_S) dt \end{aligned} \quad (44a)$$

$$A_m = e^{-(\delta+|t_S|^2)/G_S} \cdot \mathbf{I}_0(2\sqrt{\delta}|t_S|/G_S) \quad (44b)$$

where  $\mathbf{I}_l$  denotes the modified  $l$ th order Bessel function of the first kind.

2. The conditional covariance is

$$\text{cov}\{\hat{\mathbf{r}} | P_S > \delta\} = 0.5 \mathbf{V} \cdot \frac{A_v}{P_D} \quad (45)$$

where  $A_v$  is also a constant value related to output SNR.

$$\begin{aligned} A_v &= G_S \int_\delta^\infty \frac{1}{G_S} \left( \frac{t}{L|t_S|^2} \right)^{(L-1)/2} e^{-(t+L|t_S|^2)/G_S} \\ &\quad \cdot \mathbf{I}_{L-1}(2\sqrt{tL}|t_S|/G_S) t^{-1} dt \end{aligned} \quad (46a)$$

$$\mathbf{V} = \text{Re}\{\mathbf{G}_D - \mathbf{G}_{DS}G_S^{-1}\mathbf{G}_{DS}^H\}/G_S \quad (46b)$$

When the detection threshold is set to  $\delta = 0$ ,  $P_D = 1$  and  $A_m = 0$  according to (44). Then, the conditional covariance of (45) can be directly denoted by the covariance as

$$\text{cov}\{\hat{\mathbf{r}}\} = 0.5A_v \cdot \mathbf{V} \quad (47)$$

In this case, the parameter estimation covariance is determined by matrices  $\mathbf{C}$  and  $\mathbf{V}$  from (39b) and (47) as

$$\text{cov}\{\boldsymbol{\rho}\} = 0.5A_v \cdot \mathbf{C}\mathbf{V}\mathbf{C}^T \quad (48)$$

$\mathbf{V}$  can be further represented according to the weights used in (36) as

$$\mathbf{V} = \text{diag}(V_{\theta\theta}, V_{\varphi\varphi}, V_{\alpha\alpha}, V_{\beta\beta}) \quad (49)$$

$$V_{\rho\rho} = \text{Re} \left\{ \frac{\gamma^2 \bar{\mathbf{w}}_{\Delta\rho}^H \bar{\mathbf{a}} \bar{\mathbf{a}}^H \bar{\mathbf{w}}_{\Delta\rho} + \bar{\mathbf{w}}_{\Delta\rho}^H \bar{\mathbf{w}}_{\Delta\rho}}{\gamma^2 \bar{\mathbf{w}}_{\Sigma}^H \bar{\mathbf{a}} \bar{\mathbf{a}}^H \bar{\mathbf{w}}_{\Sigma} + \bar{\mathbf{w}}_{\Sigma}^H \bar{\mathbf{w}}_{\Sigma}} - \frac{(\gamma^2 \bar{\mathbf{w}}_{\Delta\rho}^H \bar{\mathbf{a}} \bar{\mathbf{a}}^H \bar{\mathbf{w}}_{\Sigma} + \bar{\mathbf{w}}_{\Delta\rho}^H \bar{\mathbf{w}}_{\Sigma})(\gamma^2 \bar{\mathbf{w}}_{\Delta\rho}^H \bar{\mathbf{a}} \bar{\mathbf{a}}^H \bar{\mathbf{w}}_{\Sigma} + \bar{\mathbf{w}}_{\Delta\rho}^H \bar{\mathbf{w}}_{\Sigma})^H}{(\gamma^2 \bar{\mathbf{w}}_{\Sigma}^H \bar{\mathbf{a}} \bar{\mathbf{a}}^H \bar{\mathbf{w}}_{\Sigma} + \bar{\mathbf{w}}_{\Sigma}^H \bar{\mathbf{w}}_{\Sigma})^2} \right\} \quad (50)$$

where  $\rho = \theta, \varphi, \alpha, \beta$ , and  $\bar{\mathbf{a}} = \bar{\mathbf{A}}(\theta, \varphi)\mathbf{p}(\alpha, \beta)$ . In the high SNR case, i.e.,  $\gamma^2 |\bar{\mathbf{a}}^H \bar{\mathbf{w}}_{\Sigma}|^2 \gg \bar{\mathbf{w}}_{\Sigma}^H \bar{\mathbf{w}}_{\Sigma}$ , (50) is simplified to

$$V_{\rho\rho} \approx \text{Re} \left\{ \frac{\bar{\mathbf{w}}_{\Delta\rho}^H \bar{\mathbf{w}}_{\Delta\rho}}{\bar{\mathbf{w}}_{\Sigma}^H \bar{\mathbf{w}}_{\Sigma}} - \left( \frac{\bar{\mathbf{w}}_{\Delta\rho}^H \bar{\mathbf{a}}}{\bar{\mathbf{w}}_{\Sigma}^H \bar{\mathbf{a}}} \right) \left( \frac{\bar{\mathbf{w}}_{\Delta\rho}^H \bar{\mathbf{a}}}{\bar{\mathbf{w}}_{\Sigma}^H \bar{\mathbf{a}}} \right)^H \left( \frac{\gamma^2 |\bar{\mathbf{w}}_{\Sigma}^H \bar{\mathbf{a}}|^2}{\bar{\mathbf{w}}_{\Sigma}^H \bar{\mathbf{w}}_{\Sigma}} + 1 \right)^{-1} \right\} \quad (51)$$

125 The second part of (51),  $\left( \frac{\gamma^2 |\bar{\mathbf{w}}_{\Sigma}^H \bar{\mathbf{a}}|^2}{\bar{\mathbf{w}}_{\Sigma}^H \bar{\mathbf{w}}_{\Sigma}} + 1 \right)^{-1}$ , is the reciprocal of sum beam output SNR.

#### 4.2. Relationship Between Estimation Error Variances and PS Factor

Firstly, the monopulse slope  $F_{\rho\rho}$  of (38) can be refined as

$$F_{\theta\theta} = \kappa_{\theta} \quad (52a)$$

$$F_{\varphi\varphi} = \kappa_{\varphi} \quad (52b)$$

$$F_{\alpha\alpha} = \frac{(\sin^2 \beta_0 - \cos^2 \beta_0)^2 z^2}{(\bar{\mathbf{w}}_{\Sigma}^H \bar{\mathbf{w}}_{\Sigma})^2} \quad (52c)$$

$$F_{\beta\beta} = \frac{z^2}{(\bar{\mathbf{w}}_{\Sigma}^H \bar{\mathbf{w}}_{\Sigma})^2} \quad (52d)$$

where

$$\kappa_{\theta} = -k_0^2 \left[ \sum_{m=1}^M (x_m \cos \theta_0 \cos \varphi_0 + y_m \cos \theta_0 \sin \varphi_0 - z_m \sin \theta_0)^2 - \left( \sum_{m=1}^M (x_m \cos \theta_0 \cos \varphi_0 + y_m \cos \theta_0 \sin \varphi_0 - z_m \sin \theta_0) \right)^2 \right] \quad (53a)$$

$$\kappa_{\varphi} = -k_0^2 \sin^2 \theta_0 \left[ \sum_{m=1}^M (-x_m \sin \varphi_0 + y_m \cos \varphi_0)^2 - \left( \sum_{m=1}^M (-x_m \sin \varphi_0 + y_m \cos \varphi_0) \right)^2 \right] \quad (53b)$$

Note that the monopulse method is normally used for a single target that falls within the 3dB beamwidth of sum beam. Similarly, the target polarization characteristic is assumed to be close to the sum beam. Therefore,  $\bar{\mathbf{a}}$  can be approximately expressed as the sum beam weight, i.e.,  $\bar{\mathbf{a}} \approx \bar{\mathbf{w}}_\Sigma$ . Then, (51) is rewritten as

$$V_{\rho\rho} = \frac{F_{\rho\rho}}{\gamma^2 \bar{\mathbf{w}}_\Sigma^H \bar{\mathbf{w}}_\Sigma + 1} \quad (54)$$

Consequently, the estimation covariance matrix of the parameter vector  $\boldsymbol{\rho}$  is rewritten by substituting (52) and (54) into (48) as

$$\text{cov}\{\boldsymbol{\rho}\} = \text{diag}(\text{var}\{\theta\}, \text{var}\{\varphi\}, \text{var}\{\alpha\}, \text{var}\{\beta\}) \quad (55a)$$

$$\text{var}\{\rho\} = \frac{A_v V_{\rho\rho}}{2F_{\rho\rho}^2} = \frac{A_v}{2F_{\rho\rho}(\gamma^2 \bar{\mathbf{w}}_\Sigma^H \bar{\mathbf{w}}_\Sigma + 1)}, \rho = \theta, \varphi, \alpha, \beta \quad (55b)$$

The variances in (55b) are further expressed separately as

$$\text{var}\{\theta\} = \frac{A_v}{2\kappa_\theta(\gamma^2 \bar{\mathbf{w}}_\Sigma^H \bar{\mathbf{w}}_\Sigma + 1)} \quad (56a)$$

$$\text{var}\{\varphi\} = \frac{A_v}{2\kappa_\varphi(\gamma^2 \bar{\mathbf{w}}_\Sigma^H \bar{\mathbf{w}}_\Sigma + 1)} \quad (56b)$$

$$\text{var}\{\alpha\} = \frac{A_v}{2\gamma^2} \cdot \frac{\bar{\mathbf{w}}_\Sigma^H \bar{\mathbf{w}}_\Sigma}{(\sin^2 \beta_0 - \cos^2 \beta_0)^2 z^2} \quad (56c)$$

$$\text{var}\{\beta\} = \frac{A_v}{2\gamma^2} \cdot \frac{\bar{\mathbf{w}}_\Sigma^H \bar{\mathbf{w}}_\Sigma}{z^2} \quad (56d)$$

where  $\bar{\mathbf{w}}_\Sigma^H \bar{\mathbf{w}}_\Sigma$  is the noise power of the normalized sum beam. The term  $\bar{\mathbf{w}}_\Sigma^H \bar{\mathbf{w}}_\Sigma / z^2$  decreases monotonically with increase of  $z^2$ , which is proved in Appendix A. Then, the variances for polarization estimations in (56c) and (56d) decrease with  $z^2$ .

For the VSA with multi feed-point ( $J > 1$ ) antennas, (56) can be simplified as

$$\text{var}\{\theta\} = \frac{A_v}{2\kappa_\theta [\gamma^2 (a + bz^2) + 1]} \quad (57a)$$

$$\text{var}\{\varphi\} = \frac{A_v}{2\kappa_\varphi [\gamma^2 (a + bz^2) + 1]} \quad (57b)$$

$$\text{var}\{\alpha\} = \frac{A_v}{2\gamma^2 (\sin^2 \beta_0 - \cos^2 \beta_0)^2} \left( b + \frac{a}{z^2} \right) \quad (57c)$$

$$\text{var}\{\beta\} = \frac{A_v}{2\gamma^2} \left( b + \frac{a}{z^2} \right) \quad (57d)$$

130 Therefore, all variances for both DOA and polarization estimations are **inversely** proportional to  $z^2$  for VSA.

### 4.3. Computational Complexity

The computational complexity comparison of the proposed GAME algorithm and the dimension-reduction MUSIC algorithm in [30] is shown in Table 1. For clarity, detailed steps of the dimension-reduction MUSIC are listed as follows.

- 135 1. Compute the covariance matrix  $\mathbf{R}_x = \mathbf{x}\mathbf{x}^H$  from the array output  $\mathbf{x}$ .
2. Obtain the noise subspace  $\mathbf{U}_N$  from  $\mathbf{R}_x$ .
3. Compute the power density spectrum function for DOA and polarization parameters according to (14) and (15) in [30], respectively.
- 140 4. Set the sample grid interval  $\theta_i$  and the times of peak searching  $G = 2 \times 180 \times 360 / (\theta_i)^2$ . Then, perform two 2-D peak searches over the whole direction and polarization domains.

The computational complexity of the GAME algorithm is much smaller than that of the dimension-reduction MUSIC algorithm. There are no calculations in the GAME algorithm regarding the covariance matrix. The target parameters can be quickly and easily estimated by comparing the outputs of the sum and difference beams.

Table 1: Comparison of computational complexity of the proposed GAME algorithm and the dimension-reduction MUSIC in [30] (/number of complex multiplications).

	Beam outputs $s_\Sigma$ and $d_\rho$	Monopulse ratio $\hat{r}$	Parameter estimation from (24)	Output covariance matrix	Noise subspace	Power density spectrum function	Peak search	Total
GAME	$5LJM$	$4L$	4					$5LJM + 4L + 4$
Dimension-Reduction MUSIC				$LJ^2M^2$	$O(J^3M^3)$	$4J^2M^2(JM - K) + O(J^3M^3)$	$O(G^3)$	$LJ^2M^2 + 4J^2M^2(JM - K) + O(J^3M^3) + O(G^3)$

## 5. Simulations and Results

145 For a fair comparison, the same microstrip patch antennas and  $5 \times 5$  planar array structure in X-band are employed in both the SSA and the VSA, as shown in Figs. 3 and 4.

The horizontal and vertical components of the vector sensor,  $\mathbf{f}_{h,vs\alpha}(\theta_k, \varphi_k)$  and  $\mathbf{f}_{v,vs\alpha}(\theta_k, \varphi_k)$  in (11), are directly obtained from ports C and D in Fig. 3(a). The multi-layer structure of each antenna is given in Fig. 3(b).

150 The scalar sensor is formed through an extra directional coupler connected to C and D shown in Fig. 3(c). If port A receives the incident signal and port B connects to the matched load, the scalar sensor is a right-handed circularly polarized antenna and the feed network  $\mathbf{N} = \text{diag}(1, -j)$ . On the other hand, if port B receives the

incident signal and port A connects to the matched load, it becomes a left-handed circularly polarized antenna and  $\mathbf{N} = \text{diag}(1, j)$ . The structure parameters of the dual-circularly polarized antenna are listed in Table 2. In the following simulations, the right-handed circularly polarized antenna is employed.

Three inter-element spacings,  $d = 0.5\lambda$ ,  $0.53\lambda$  and  $0.56\lambda$ , are employed. Both the SSA and the VSA are modeled by the EM full-wave simulation software *Ansoft HFSS* [43]. The corresponding horizontal and vertical components of the active element patterns are directly exported from port C and D of Fig. 3(a) for the VSA and port A of Fig. 3(c) for the SSA. The number of Monte-Carlo experiments is set to  $M_C = 1000$ .

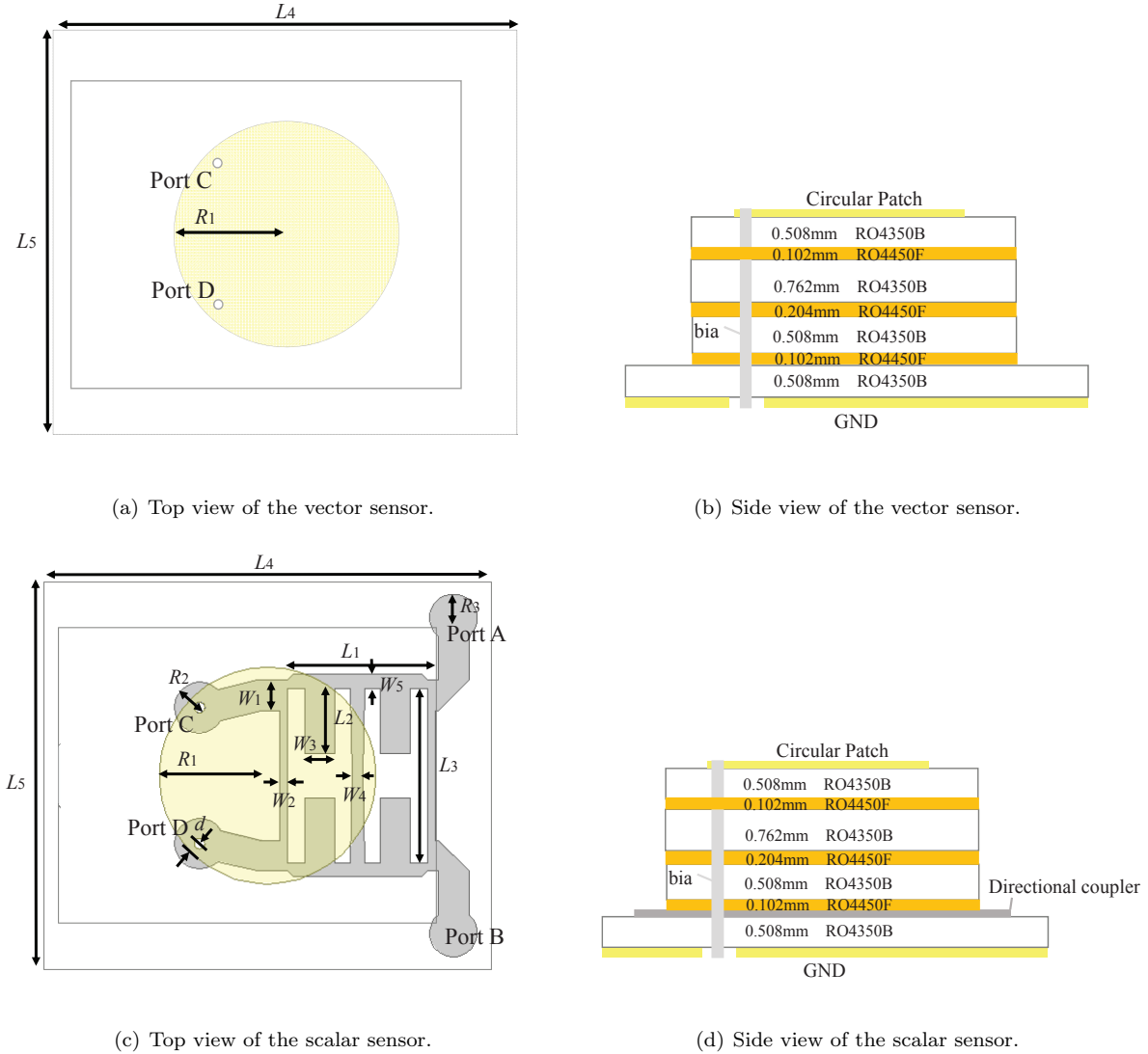
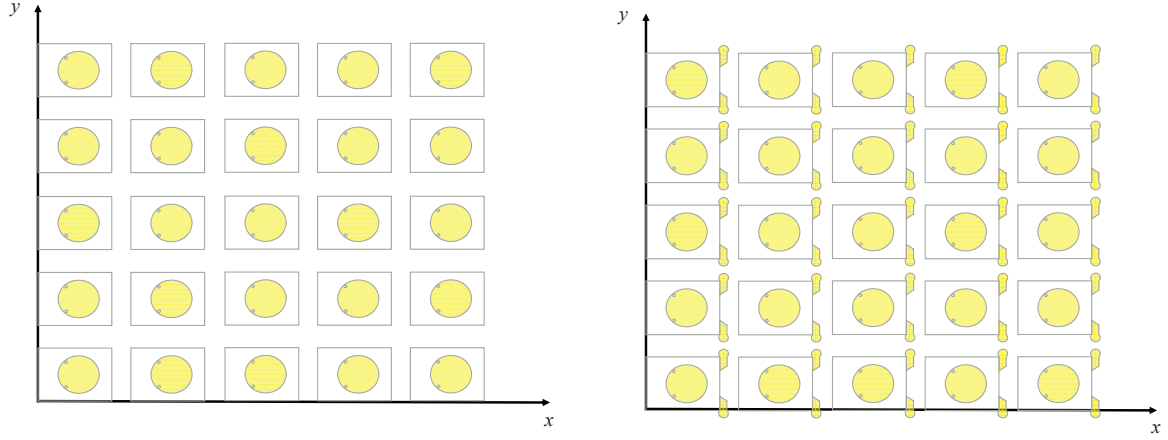


Figure 3: Structure of the employed microstrip patch antenna.

### 5.1. Array Polarization Sensitivity

The degree of PS in the spatial domain of the arrays in Fig. 4 under different inter-element spacings is presented in Fig. 5, where the azimuth angle is fixed at  $\varphi = 0^\circ$  and the elevation angle varies from  $0^\circ$  to  $60^\circ$ . In general, the PS of the VSA is much larger than that of the SSA.



(a) The VSA.

(b) The SSA.

Figure 4: Planar rectangular arrays with 25 microstrip patch antennas.

Table 2: Parameters of the dual-circular polarized antenna.

Parameter	Value(mm)	Parameter	Value(mm)
$R_1$	3.8	$W_1$	1.1
$R_2$	0.85	$W_2$	0.3
$R_3$	0.9	$W_3$	1.0
$L_1$	4.6	$W_4$	0.4
$L_2$	2.4	$W_5$	0.5
$L_3$	6.2	$d$	0.2

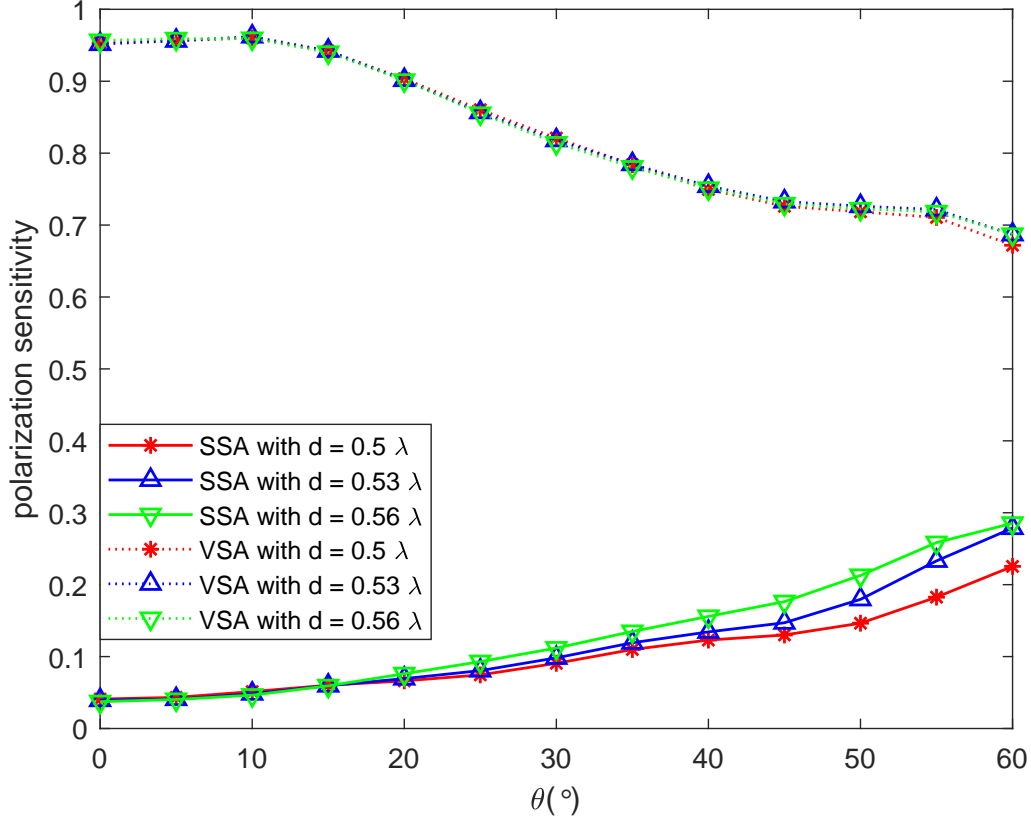


Figure 5: PS of the SSA/VSA.

For the SSA,  $z(\theta, \varphi)$  is relatively small. As described in Section 2.2, the PS of the SSA comes from the diversities of the horizontal and vertical electric field components among different antennas due to the presence of MC. For the same inter-element spacing  $d$ , a larger  $\theta$  leads to greater electric field diversities among antennas. That's the reason why  $z(\theta, \varphi)$  increases with  $\theta$  in Fig. 5. However, for the same  $\theta$ , a smaller  $d$  means larger MC, and the distortion of both electric field components of all antennas becomes serious. But  $z$  depends on the difference or diversity among antennas, not directly on distortion, and interestingly larger distortion does not lead to greater diversity. On the contrary, the gain consistency among antennas is improved to certain degree as  $d$  decreases. Thus,  $z$  decreases with a smaller  $d$ .

For the VSA,  $z(\theta, \varphi)$  is generally large, close to 1, especially when  $\theta$  is near the boresight. As analyzed in Section 2.3, the PS of the VSA depends on the gain consistency of the two orthogonal electric field components. Therefore, the difference of the inter-element spacing  $d$  does not cause a significant effect on  $z$ . However, the gain inconsistency between orthogonal channels of each antenna will deteriorate as  $\theta$  increases, resulting in a decrease in  $z$ .

## 5.2. Performance Comparison

In this example, the proposed GAME is compared with the MUSIC algorithm in [30]. The Cramer-Rao bound (CRB) will be given as a benchmark when evaluating the performance of two estimators. Although the

monopulse estimator is nonlinear, the CRB is still valid because the unbiasedness is achieved asymptotically under the circumstance of large snapshots  $L$  or high SNR. The deterministic CRB is presented in [44]

$$\text{CRB} = \frac{\sigma^2 \mathbf{I}_{JM}}{2L \cdot \text{SNR}} \left[ \text{Re} \left\{ \mathbf{A}_\rho^H \cdot \left[ \mathbf{I}_{JM} - \frac{\mathbf{a}\mathbf{a}^H}{\mathbf{a}^H \mathbf{a}} \right] \cdot \mathbf{A}_\rho \right\} \right]^{-1} \quad (58)$$

where  $\mathbf{A}_\rho$  is the derivative matrix of  $\mathbf{a}$  as

$$\mathbf{A}_\rho = \left( \frac{\partial \mathbf{a}}{\partial \theta}, \frac{\partial \mathbf{a}}{\partial \varphi}, \frac{\partial \mathbf{a}}{\partial \alpha}, \frac{\partial \mathbf{a}}{\partial \beta} \right). \quad (59)$$

The parameter estimation performance is evaluated in terms of the root mean square error (RMSE) as  $\text{RMSE} = \sqrt{\frac{1}{M_C} \sum_i^{M_C} (\hat{\rho}_i - \rho)^2}$ , where  $\hat{\rho}_i$  is the parameter estimate at the  $i$ th run. The SSA with  $d = 0.5\lambda$ , and a signal with polarization  $(\alpha_t, \beta_t) = (60^\circ, -10^\circ)$  from direction  $(\theta_t, \varphi_t) = (30^\circ, 45^\circ)$  are considered. The RMSEs and variances versus input SNR under different numbers of snapshots  $L$  are shown in Figs. 6 and 7. The averaged monopulse ratio in (27) is used under the case of multiple snapshots.

The performance comparisons are illustrated in Fig. 6 when the parameters of the sum beam match with the incident signal. In this case, the mean of the GAME estimator can be obtained from (39a) as  $E = 0$ , i.e., the RMSE is equivalent to the variance. The proposed algorithm outperforms the MUSIC algorithm both in robustness and parameter estimation performance at different  $L$ , owing to the property of *monopulse* to fully use the array gain. The MUSIC algorithm in [30] can give satisfactory results only when accurate noise subspace is estimated, such as in relatively high SNR and for a large  $L$ .

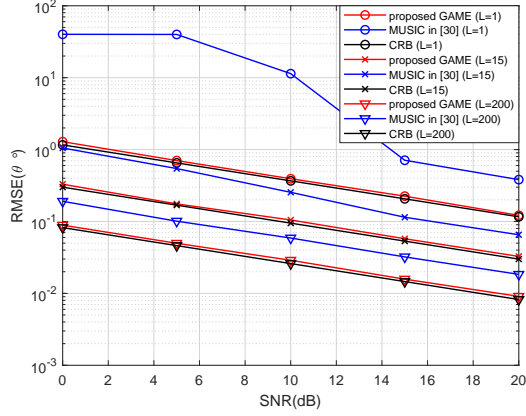
Fig. 7 shows the performance when the parameters of the sum beam mismatch with the incident signal. In this case, the GAME estimator is biased. The variances of the proposed algorithm remain almost the same as those in Fig. 6. However, the RMSEs decrease at high SNR and large  $L$ . This is because when SNR or  $L$  increases, the mean error caused by biased estimation gradually occupies the main component of the RMSE.

We can see from Figs. 6 and 7 that when  $L = 1$ , the RMSE of MUSIC algorithm is much higher than the GAME algorithm even at high SNR due to the estimation error of the noise subspace.

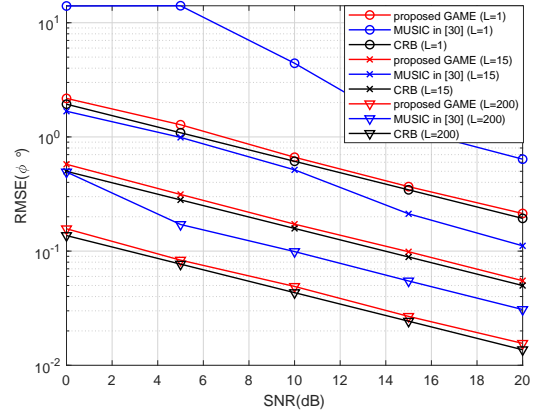
### 5.3. RMSE versus $z(\theta, \varphi)$

Firstly, the RMSE of the SSA is evaluated using a signal with polarization  $(\alpha_t, \beta_t) = (60^\circ, -10^\circ)$  from direction  $(\theta_t, \varphi_t) = (35^\circ, 0^\circ)$ , and  $L = 1$ . The PS factors  $z(35^\circ, 0^\circ)$  for  $d = 0.5\lambda, 0.53\lambda$ , and  $0.56\lambda$  are 0.11, 0.12, and 0.135, respectively. The RMSEs versus input SNR when the signal parameters match with the sum beam are shown in Fig. 8. The statistical analysis results represented by the asterisk are completely consistent with the theoretical values calculated by (56). The strict monotonic relationship between RMSEs of polarization and  $r$  matches the analysis in Section 4.2.

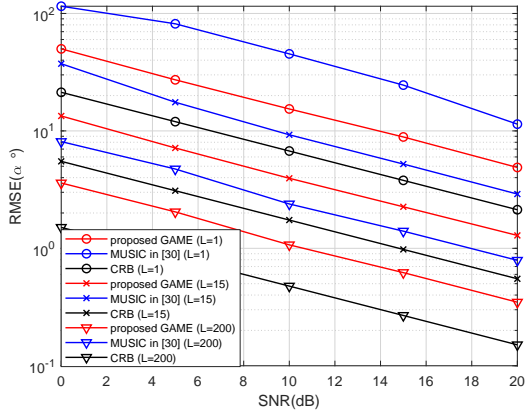
Next, the VSA is considered. Since the PS factors of the VSAs with different  $d$  are similar to each other at the same direction shown in Fig. 5,  $z(\theta, \varphi)$  is mainly affected by the incident signal directions. Thus, three directions are considered when  $d = 0.5\lambda$ , i.e.,  $z(10^\circ, 0^\circ) = 0.96$ ,  $z(20^\circ, 0^\circ) = 0.9$ , and  $z(30^\circ, 0^\circ) = 0.81$ . The RMSE results versus input SNR are shown in Fig. 9, where  $L = 1$  and  $(\alpha_t, \beta_t) = (60^\circ, -10^\circ)$ . The parameters of these sum beams all match with the incident signals. Similarly, the statistical analysis results represented by the asterisk



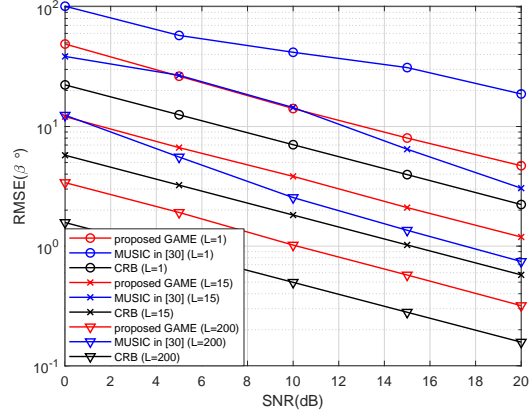
(a) RMSE of  $\theta$  versus SNR.



(b) RMSE of  $\varphi$  versus SNR.

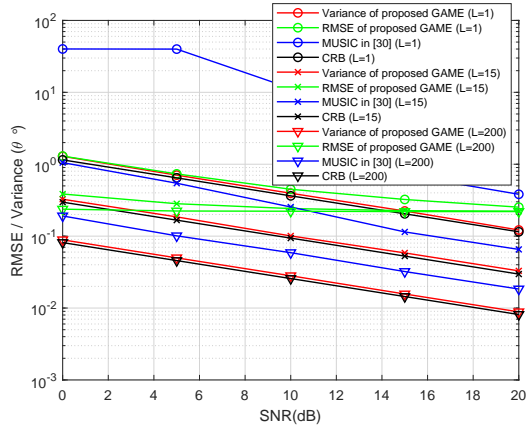


(c) RMSE of  $\alpha$  versus SNR.

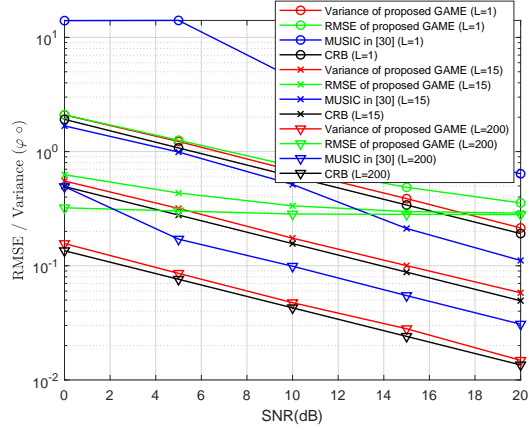


(d) RMSE of  $\beta$  versus SNR.

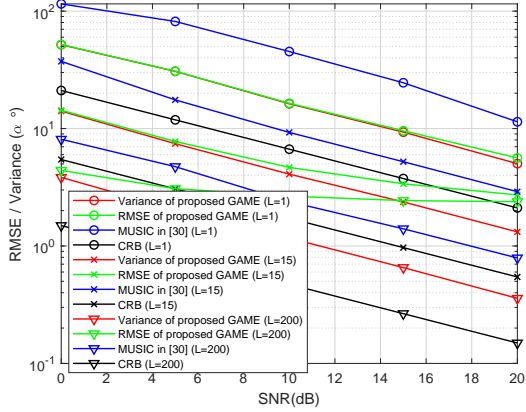
Figure 6: RMSEs versus SNR when the parameters of the sum beam  $(\theta_0, \varphi_0, \alpha_0, \beta_0) = (30^\circ, 45^\circ, 60^\circ, -10^\circ)$  match with the signal.



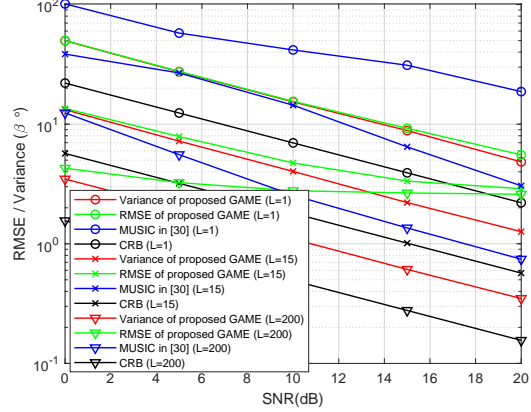
(a) RMSE and variance of  $\theta$  versus SNR.



(b) RMSE and variance of  $\varphi$  versus SNR.

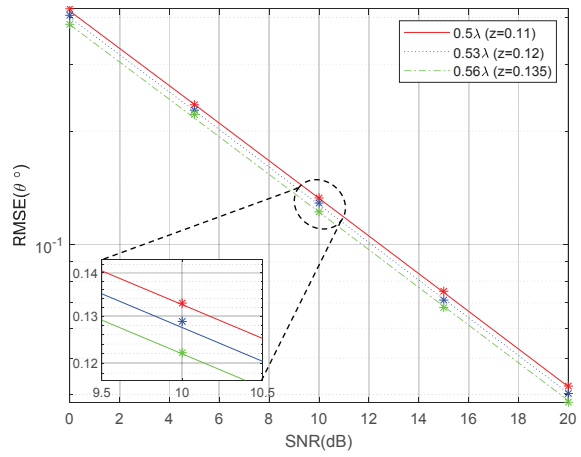


(c) RMSE and variance of  $\alpha$  versus SNR.

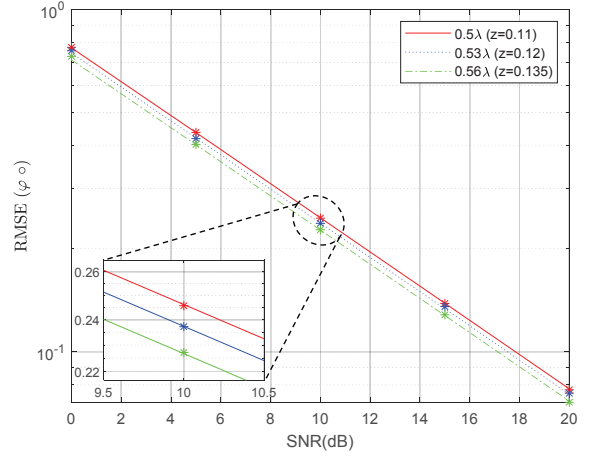


(d) RMSE and variance of  $\beta$  versus SNR.

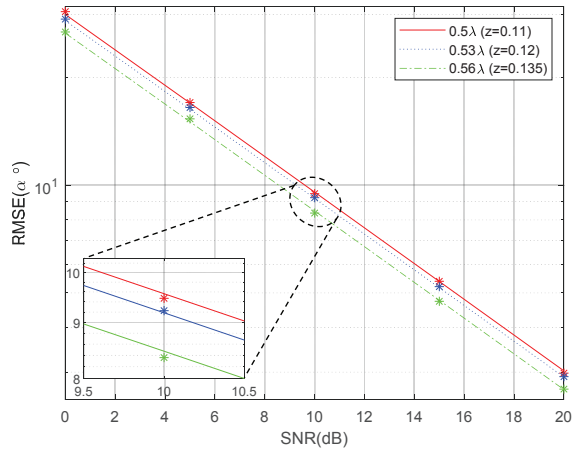
Figure 7: RMSEs and variances versus SNR when the parameters of the sum beam  $(\theta_0, \varphi_0, \alpha_0, \beta_0) = (29^\circ, 46^\circ, 65^\circ, -10^\circ)$  mismatch with the signal.



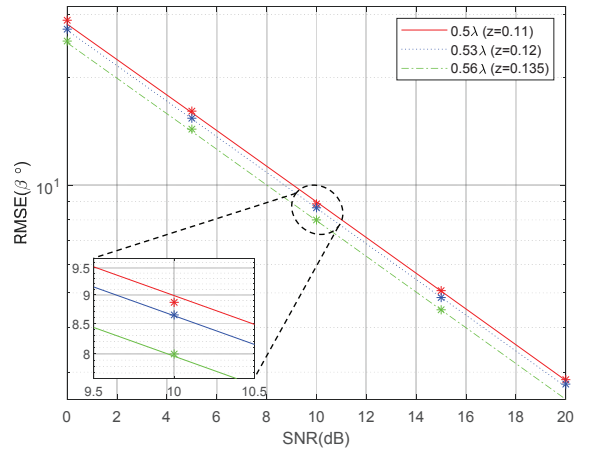
(a) RMSE of  $\theta$  versus SNR.



(b) RMSE of  $\varphi$  versus SNR.



(c) RMSE of  $\alpha$  versus SNR.



(d) RMSE of  $\beta$  versus SNR.

Figure 8: RMSEs versus SNR based on the SSA.

are almost completely overlapped with the theoretical values calculated by (57). We can also see that the RMSEs of polarization decrease monotonically with  $z$ , consistent with the analysis in Section 4.2.

Finally, compared with Figs. 8 and 9, the DOA RMSEs of the VSA are close to those of the SSA for almost the same array gain in both arrays. However, the polarization RMSEs of the VSA is much better than those of the SSA for its superior polarization diversity.

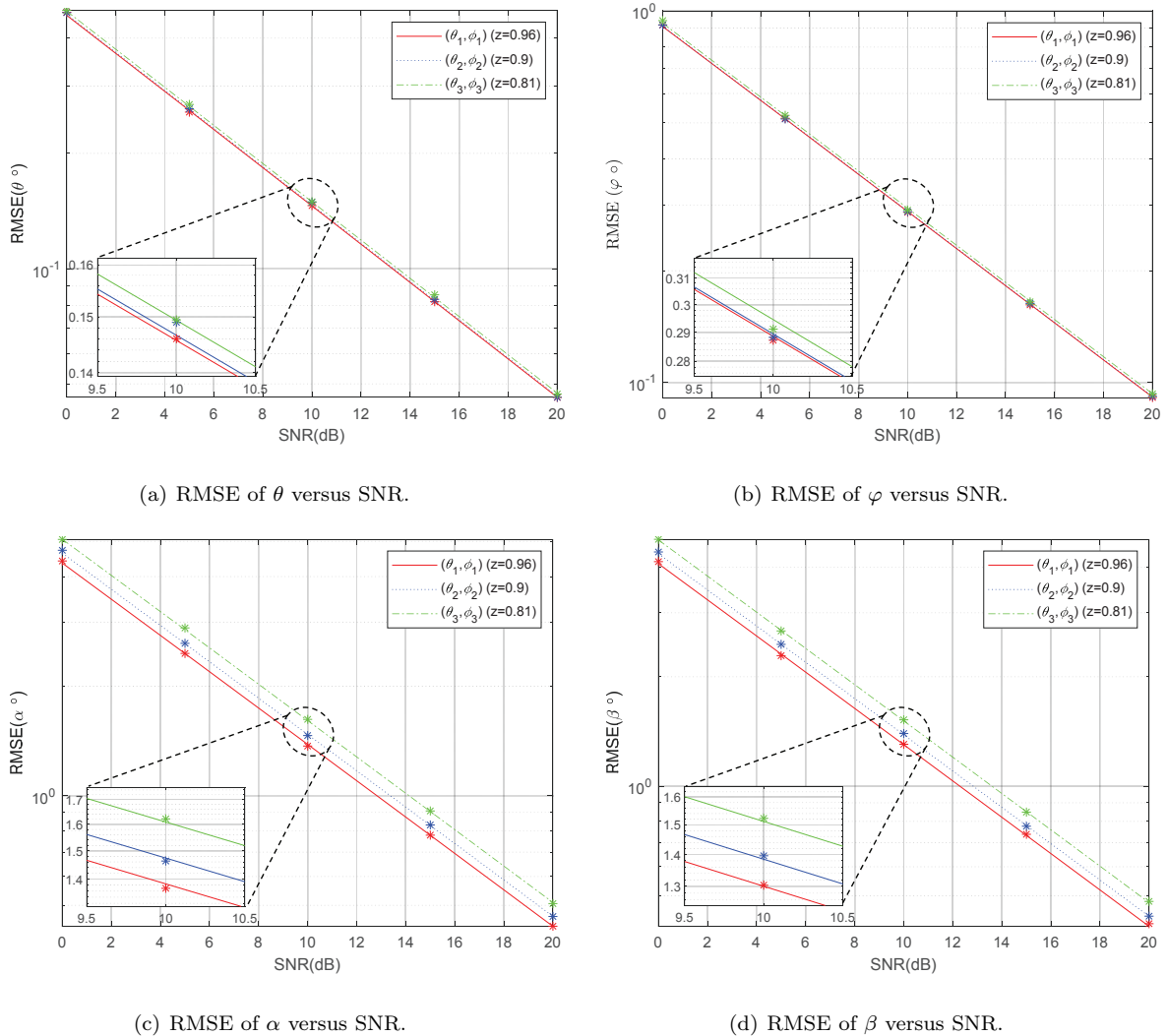


Figure 9: RMSEs versus SNR based on the VSA.

## 6. Conclusion

In this paper, the joint DOA and polarization estimation problem was studied and a generalized monopulse estimation method was proposed for both VSAs and SSAs. The proposed GAME algorithm is computationally efficient with higher estimation accuracy compared with existing subspace-based algorithms. The closed-form expressions of estimation error variances of GAME were derived, and the polarization estimation variance was proved to be proportional to the reciprocal of the square of the PS factor  $z$ .

In addition, VSAs and SSAs with polarization sensitivity are unified under the same framework of PSAs in this paper. The PS of SSA originating from the mutual coupling effect is analyzed in detail. The *unpredictable* polarization diversity associated with SSAs could be obtained by EM full-wave simulation softwares in advance. One interesting phenomenon is that, although the MC effect is commonly considered as a disadvantage in antenna array design, the resultant PS offers a good property to achieve effective polarization estimation which is traditionally deemed impossible with such SSAs.

## Appendix A. Proof of the Monotonicity Term in (56)

First, according to (36a), the noise power  $\bar{\mathbf{w}}_\Sigma^H \bar{\mathbf{w}}_\Sigma$  can be decomposed into the polarization vector and the array manifold matrix as

$$\bar{\mathbf{w}}_\Sigma^H \bar{\mathbf{w}}_\Sigma = \mathbf{p}^H \bar{\mathbf{A}}^H \bar{\mathbf{A}} \mathbf{p} = \mathbf{p}^H \bar{\mathbf{B}} \mathbf{p} \quad (\text{A.1})$$

The Hermitian positive definite matrix  $\bar{\mathbf{B}}$  can be represented as

$$\bar{\mathbf{B}} = \bar{\lambda}_1 \mathbf{x}_1 \mathbf{x}_1^H + \bar{\lambda}_2 \mathbf{x}_2 \mathbf{x}_2^H \quad (\text{A.2})$$

where  $\mathbf{x}_1, \mathbf{x}_2 \in \mathbb{C}^{2 \times 1}$  are the orthogonal unit eigenvectors corresponding to the larger eigenvalue  $\bar{\lambda}_1$  and smaller eigenvalue  $\bar{\lambda}_2 = z^2$ , respectively. The larger the PS factor, the larger  $\bar{\lambda}_2$ . Then,  $\bar{\mathbf{w}}_\Sigma^H \bar{\mathbf{w}}_\Sigma$  can be written as

$$\bar{\mathbf{w}}_\Sigma^H \bar{\mathbf{w}}_\Sigma = \bar{\lambda}_1 \mathbf{p}^H \mathbf{x}_1 \mathbf{x}_1^H \mathbf{p} + \bar{\lambda}_2 \mathbf{p}^H \mathbf{x}_2 \mathbf{x}_2^H \mathbf{p} \quad (\text{A.3})$$

where  $\mathbf{p}^H \mathbf{x}_1 \mathbf{x}_1^H \mathbf{p} + \mathbf{p}^H \mathbf{x}_2 \mathbf{x}_2^H \mathbf{p} = 1$  with  $\mathbf{p}^H \mathbf{p} = 1$ . Thus,  $\bar{\mathbf{w}}_\Sigma^H \bar{\mathbf{w}}_\Sigma / z^2$  can be rewritten as

$$\begin{aligned} \frac{\bar{\mathbf{w}}_\Sigma^H \bar{\mathbf{w}}_\Sigma}{\bar{\lambda}_2} &= \frac{\bar{\lambda}_1 \mathbf{p}^H \mathbf{x}_1 \mathbf{x}_1^H \mathbf{p} + \bar{\lambda}_2 \mathbf{p}^H \mathbf{x}_2 \mathbf{x}_2^H \mathbf{p}}{\bar{\lambda}_2} \\ &= \frac{\bar{\lambda}_1}{\bar{\lambda}_2} \mathbf{p}^H \mathbf{x}_1 \mathbf{x}_1^H \mathbf{p} + \mathbf{p}^H \mathbf{x}_2 \mathbf{x}_2^H \mathbf{p} \\ &= \left( \frac{1}{\bar{\lambda}_2} - 1 \right) \mathbf{p}^H \mathbf{x}_1 \mathbf{x}_1^H \mathbf{p} + 1. \end{aligned} \quad (\text{A.4})$$

Both terms of  $(1/\bar{\lambda}_2 - 1) \geq 0$  and  $\mathbf{p}^H \mathbf{x}_1 \mathbf{x}_1^H \mathbf{p} > 0$  decrease monotonically with increasing  $\bar{\lambda}_2$ . This completes the proof.

## Acknowledgment

This work is supported by the Strengthening Foundation Program Fund of China under Grant 2019-JCJQ-JJ-366, by the National Natural Science Foundation of China under Grant 61971224, and by Postgraduate Research & Practice Innovation Program of Jiangsu Province under Grant KYCX20-0282.

## References

- [1] A. J. Weiss, B. Friedlander, Performance analysis of diversely polarized antenna arrays, IEEE Transactions on Signal Processing 39 (7) (1991) 1589–1603.

- [2] M. R. Andrews, P. P. Mitra, R. Decarvalho, Tripling the capacity of wireless communications using electromagnetic polarization, *Nature* 409 (6818) (2001) 316–318.
- [3] W. Liu, Channel equalization and beamforming for quaternion-valued wireless communication systems, *Journal of the Franklin Institute* 354 (18) (2017) 8721 – 8733. doi:<https://doi.org/10.1016/j.jfranklin.2016.10.043>.
- [4] Kah-Chye Tan, Kwok-Chiang Ho, A. Nehorai, Uniqueness study of measurements obtainable with arrays of electromagnetic vector sensors, *IEEE Transactions on Signal Processing* 44 (4) (1996) 1036–1039.
- [5] A. Nehorai, E. Paldi, Vector-sensor array processing for electromagnetic source localization, *IEEE Transactions on Signal Processing* 42 (2) (1994) 376–398.
- [6] K. Wong, M. Zoltowski, Closed-form direction finding and polarization estimation with arbitrarily spaced electromagnetic vector-sensors at unknown locations, *IEEE Transactions on Antennas and Propagation* 48 (5) (2000) 671–681. doi:[10.1109/8.855485](https://doi.org/10.1109/8.855485).
- [7] M. Zoltowski, K. Wong, Esprit-based 2-d direction finding with a sparse uniform array of electromagnetic vector sensors, *IEEE Transactions on Signal Processing* 48 (8) (2000) 2195–2204. doi:[10.1109/78.852000](https://doi.org/10.1109/78.852000).
- [8] K.-C. Ho, K.-C. Tan, A. Nehorai, Estimating directions of arrival of completely and incompletely polarized signals with electromagnetic vector sensors, *IEEE Transactions on Signal Processing* 47 (10) (1999) 2845–2852. doi:[10.1109/78.790664](https://doi.org/10.1109/78.790664).
- [9] K.-C. Tan, K.-C. Ho, A. Nehorai, Uniqueness study of measurements obtainable with arrays of electromagnetic vector sensors, *IEEE Transactions on Signal Processing* 44 (4) (1996) 1036–1039. doi:[10.1109/78.492566](https://doi.org/10.1109/78.492566).
- [10] H. Ma, H. Tao, H. Kang, Mixed far-field and near-field source localization using a linear electromagnetic-vector-sensor array with gain/phase uncertainties, *IEEE Access* (2020) 1–1doi:[10.1109/ACCESS.2020.2981483](https://doi.org/10.1109/ACCESS.2020.2981483).
- [11] Z. Zhang, J. He, T. Shu, W. Yu, Successive method for angle-polarization estimation with vector-sensor array, *IEEE Sensors Letters* 2 (1) (2018) 1–4. doi:[10.1109/LENS.2018.2808263](https://doi.org/10.1109/LENS.2018.2808263).
- [12] S. C. Gao, L. W. Li, T. S. Yeo, M. S. Leong, Low cost, dual linearly polarised microstrip patch array, *IEE Proceedings - Microwaves, Antennas and Propagation* 148 (1) (2001) 21–24.
- [13] J. Li, D. Wu, G. Zhang, Y. Wu, C. Mao, A left/right-handed dual circularly-polarized antenna with duplexing and filtering performance, *IEEE Access* 7 (2019) 35431–35437.
- [14] H. Krim, M. Viberg, Two decades of array signal processing research: the parametric approach, *IEEE Signal Processing Magazine* 13 (4) (1996) 67–94.
- [15] B. Friedlander, Antenna array manifolds for high-resolution direction finding, *IEEE Transactions on Signal Processing* 66 (4) (2018) 923–932.

- [16] H. L. V. Trees, *Detection, Estimation, and Modulation Theory, Optimum Array Processing*, Publishing House of Electronics Industry, 2013.
- [17] B. Friedlander, Polarization sensitivity of antenna arrays, *IEEE Transactions on Signal Processing* 67 (1) (2019) 234–244. 270
- [18] I. Gupta, A. Ksienski, Effect of mutual coupling on the performance of adaptive arrays, *IEEE Transactions on Antennas and Propagation* 31 (5) (1983) 785–791.
- [19] H. Steyskal, J. S. Herd, Mutual coupling compensation in small array antennas, *IEEE Transactions on Antennas and Propagation* 38 (12) (1990) 1971–1975.
- [20] A. H. Mohammadian, N. M. Martin, D. W. Griffin, A theoretical and experimental study of mutual coupling in microstrip antenna arrays, *IEEE Transactions on Antennas and Propagation* 37 (10) (1989) 1217–1223. 275
- [21] Y. Hua, A pencil-music algorithm for finding two-dimensional angles and polarizations using crossed dipoles, *IEEE Transactions on Antennas and Propagation* 41 (3) (1993) 370–376.
- [22] K. T. Wong, M. Zoltowski, Self-initiating music-based direction finding and polarization estimation in spatio-polarizational beamspace, *IEEE Transactions on Antennas and Propagation* 48 (8) (2000) 1235–1245. doi:10.1109/8.884492. 280
- [23] J. Li, Direction and polarization estimation using arrays with small loops and short dipoles, *IEEE Transactions on Antennas and Propagation* 41 (3) (1993) 379–387.
- [24] M. Zoltowski, K. Wong, Esprit-based 2-d direction finding with a sparse uniform array of electromagnetic vector sensors, *IEEE Transactions on Signal Processing* 48 (8) (2000) 2195–2204. doi:10.1109/78.852000. 285
- [25] T. Ahmed, Z. Xiaofei, Z. Wang, P. Gong, Rectangular array of electromagnetic vector sensors: tensor modelling/decomposition and doa-polarisation estimation, *IET Signal Processing* 13 (7) (2019) 689–699.
- [26] X. Lan, W. Liu, H. Y. T. Ngan, Joint 4-D DOA and polarization estimation based on linear tripole arrays, in: *22nd International Conference on Digital Signal Processing (DSP)*, 2017, pp. 1–5.
- [27] H. Jin, L. Zhong, Computationally efficient 2D direction finding and polarization estimation with arbitrarily spaced electromagnetic vector sensors at unknown locations using the propagator method, *Digital Signal Processing* 19 (3) (2009) 491–503. 290
- [28] S. Miron, N. Le Bihan, J. I. Mars, Quaternion-MUSIC for vector-sensor array processing, *IEEE Transactions on Signal Processing* 54 (4) (2006) 1218–1229.
- [29] X.-F. Gong, Z.-W. Liu, Y.-G. Xu, Coherent source localization: Bicomplex polarimetric smoothing with electromagnetic vector-sensors, *IEEE Transactions on Aerospace and Electronic Systems* 47 (3) (2011) 2268–2285. doi:10.1109/TAES.2011.5937301. 295

- [30] M. Dai, X. Ma, W. Liu, W. Sheng, Polarization parameters estimation with scalar sensor arrays, in: International Conference on Acoustics, Speech and Signal Processing (ICASSP), 2020, pp. 4667–4671.
- 300 [31] U. Nickel, Overview of generalized monopulse estimation, *IEEE Aerospace and Electronic Systems Magazine* 21 (6) (2006) 27–56.
- [32] Kai-Bor Yu, D. J. Murrow, Adaptive digital beamforming for angle estimation in jamming, *IEEE Transactions on Aerospace and Electronic Systems* 37 (2) (2001) 508–523.
- [33] U. Nickel, Performance of corrected adaptive monopulse estimation, *IEE Proceedings - Radar, Sonar and Navigation* 146 (1) (1999) 17–24.
- 305 [34] Y. Zhang, H. Sun, X. Xu, Q. H. Liu, Amplitude angle monopulse estimation for the four-channel hybrid polarimetric radar system, *IEEE Antennas and Wireless Propagation Letters* 16 (2017) 2889–2893. doi:10.1109/LAWP.2017.2751298.
- [35] Y. Lu, J. Ma, J. Zhou, L. Shi, Adaptive polarization-constrained monopulse approach for dual-polarization array, *IEEE Antennas and Wireless Propagation Letters* 20 (3) (2021) 289–292. doi:10.1109/LAWP.2020.3047684.
- 310 [36] Z. Zhang, G. Zhao, B. Liu, H. Sun, X. Lv, Research and design of two-dimensional monopulse radar system with instantaneous polarization measurement capability, in: Asia-Pacific Microwave Conference 2011, 2011, pp. 1366–1369.
- [37] N. Yang, G. Q. Zhao, L. Shi, H. J. Sun, Reconfigurable array based on dual-polarization multilayer micro-strip patch antenna for polarization detector applications, in: 2013 IEEE INTERNATIONAL CONFERENCE ON MICROWAVE TECHNOLOGY COMPUTATIONAL ELECTROMAGNETICS, 2013, pp. 232–235. doi:10.1109/ICMTCE.2013.6812440.
- 315 [38] R. Shirvany, M. Chabert, J.-Y. Tournet, Estimation of the degree of polarization for hybrid/compact and linear dual-pol sar intensity images: Principles and applications, *IEEE Transactions on Geoscience and Remote Sensing* 51 (1) (2013) 539–551. doi:10.1109/TGRS.2012.2202242.
- [39] C. A. Balanis, Antenna theory: Analysis and design, *IEEE Antennas & Propagation Society Newsletter* 24 (6) (2003) 28–29.
- [40] B. Fuchs, J. J. Fuchs, Optimal polarization synthesis of arbitrary arrays with focused power pattern, *IEEE Transactions on Antennas and Propagation* 59 (12) (2011) 4512–4519.
- 325 [41] J. Xiao, A. Nehorai, Optimal polarized beam pattern synthesis using a vector antenna array, *IEEE Transactions on Signal Processing* 57 (2) (2009) 576–587.
- [42] U. Nickel, Monopulse estimation with subarray-adaptive arrays and arbitrary sum and difference beams, *IEE Proceedings - Radar, Sonar and Navigation* 143 (4) (1996) 232–238.

- 330 [43] A. Corporation, Hfss, Suite v15, Pittsburg (PA), USA.
- [44] A. Dogandzic, A. Nehorai, Cramer-rao bounds for estimating range, velocity, and direction with an active array, *IEEE Transactions on Signal Processing* 49 (6) (2001) 1122–1137.